Tectonophysics 857 (2023) 229853

Contents lists available at ScienceDirect

Tectonophysics

journal homepage: www.elsevier.com/locate/tecto

A multi-scale approach to the recent activity of the Stradella thrust in the seismotectonic context of the Emilia Arc (northwestern Italy)

Alessandro Tibaldi [a,b,*], Rita de Nardis [c,b], Patrizio Torrese [d,b], Sofia Bressan [a], Martina Pedicini [a], Donato Talone [b,c], Fabio L. Bonali [a,b], Noemi Corti [a], Elena Russo [a,b], Giusy Lavecchia [c,b]

[a] Department of Earth and Environmental Sciences, University of Milan-Bicocca, Milan, Italy
[b] CRUST-Interuniversity Center for 3D Seismotectonics with Territorial Applications, Chieti, Italy
[c] Department of Psychological Sciences, Health and Territory, University of the Studies "G. d'Annunzio", Chieti, Italy
[d] Department of Earth and Environmental Sciences, University of Pavia, Italy

ARTICLE INFO

Keywords:
Holocene thrust
Geoelectrical survey
3D fault model
Seismotectonics
Apennines
Italy

ABSTRACT

The frontal thrusts and folds of the northern Apennines - Italy - are mainly covered under the alluvial deposits of the Po Plain. Some of these structures show geological evidence of Late Quaternary activity, thus posing the need for an accurate seismic hazard assessment due to widespread housing settlements, industries, lifeline infrastructures, and large towns. We present new morphostructural, geophysical, and seismological data to discuss the recent activity of the Broni-Sarmato fault, an 18 km-long outcropping section of the north-verging Stradella thrust, located 50 km south of Milan, along the Pede-Apennine thrust front (PTF) in the rear of the Emilia Arc thrust system. The new geoelectrical surveys across the fault scarp show deformation of the shallow deposits. The outcropping deformations, with a fault scarp ranging up to 25.8 m, are investigated within the seismotectonic framework of the PTF and the Emilia Arc. The analysis of the associated seismicity and new focal mechanisms highlight two seismogenic contractional volumes dipping at low-angle southwest-ward, at upper (<12 km) and lower crustal depths (~20–30 km). The shallow seismicity partially illuminates the Stradella thrust and its along-strike southeastward prosecution along the extent of the Stradella-Salsomaggiore Arc. Subordinately, it also illuminates some of the Emilia Arc thrust planes. The deeper seismogenic volume shows large patches of the basal thrust of the Emilia Arc fault system. We interpret the above multi-scale data as evidence of ongoing tectonic activity of the outer fronts of the Emilia Arc under a regional NNE-oriented compressional stress field, with some evidence of thrust involvement along the Pede-Apennine front. In our 3D fault-model reconstruction, all the analyzed thrust structures appear as expressions of a thick-skinned deformation that controls earthquake release at different structural levels.

1. Introduction

Investigating active tectonics and structural style of potentially-seismogenic structures at the outer front of active orogenic belts is particularly challenging when the frontal structures are buried and slowly deforming. Moreover, correlating the seismicity to the tectonics structures is not straightforward when ruptures prevalently occur at seismogenic layers that are several kilometers deep (e.g., Ito, 1999; Lavecchia et al., 2003; Watts and Burov, 2003; Turrini et al., 2015; Tsereteli et al., 2016; Ferrarini et al., 2021). Nevertheless, the complex seismotectonic framework, above described, may be well recognized in the blind fold-and-thrust belts surrounding the Padanian foreland in Northern Italy and developing across one of the most populated and industrialized Italian region (Lavecchia et al., 2003; Boncio and Bracone, 2009; Visini et al., 2010; Boccaletti et al., 2011; Bonini, 2013; Turrini et al., 2015; Vannoli et al., 2015; Martelli et al., 2017) (Fig.1).

The Alps and the Apennines are the results of the Europe-Africa still ongoing collision, occurring at a rate of 6–8 mm/yr (DeMets et al., 1990, 1994; Mazzoli and Helman, 1994). The convergence is accommodated within a broad plate boundary zone characterized by diffuse seismicity (Chiarabba et al., 2005; Mazzoli et al., 2015) and a complex deformation field (Vannoli et al., 2015).

* Corresponding author at: Department of Earth and Environmental Sciences, University of Milan-Bicocca, Milan, Italy
E-mail address: alessandro.tibaldi@unimib.it (A. Tibaldi).

https://doi.org/10.1016/j.tecto.2023.229853
Received 2 November 2022; Received in revised form 16 March 2023; Accepted 6 April 2023
Available online 23 April 2023

In the Northern Apennines, convergence is accommodated by thrusting and folding (Benedetti et al., 2000, 2003; Burrato et al., 2003; Basili and Barba, 2007; Picotti and Pazzaglia, 2008; Wilson et al., 2009; Boccaletti et al., 2011; Zuffetti and Bersezio, 2020; Lavecchia et al., 2021), which also involved a thick pile (locally up to 7–8 km) of Pliocene-Pleistocene deposits. Although the deformation is mainly accommodated by blind structures, the characteristic fold-and-thrust geometry is well known due to extensive hydrocarbon exploration consisting of regional studies based on industrial seismic reflection profiles and deep well logs (Pieri and Groppi, 1981; Cassano et al., 1986; Cazzini et al., 2015; Fantoni and Franciosi, 2010; Ghielmi et al., 2010, 2013; Turrini et al., 2015 and references therein).

These regional seismic profiles allow insights into the crustal structure, but they lose resolution when approaching the near-surface zone, corresponding to the last hundreds of meters. Moreover, at a shallow level in the Po Plain, the deposits are very young; thus, they have recorded lower amounts of deformation, possibly at the limit of the seismic resolution. Generally, the investigated crustal succession is made of deposits older than the Late Pleistocene, preventing relying on the offset of young deposits.

Also, due to the relatively poor historical seismicity along the Northern Apennine outer fronts (Rovida et al., 2022), the evidence of activity in late Quaternary times has long been questioned until the Emilia 2012 (M_W 6.1) thrust sequence that definitively demonstrated the ongoing compressional activity of the Ferrara Arc and its capability of releasing destructive earthquakes (Lavecchia et al., 2015; de Nardis et al., 2014; Govoni et al., 2014; Vannoli et al., 2015) (Fig.1).

The seismotectonic potential of the Emilia Arc, located west of the Ferrara Arc, is also poorly defined. Earthquakes from 1000 to 2020 CE highlight a modest seismic activity with events up to ca. M 5.0 and only in correspondence of the arc's western and eastern lateral segments (Rovida et al., 2022) (Fig.1). The seismicity is mainly concentrated southward of the inner thrust Pede-Apennine Thrust Front (PTF, sensu Boccaletti et al., 1985), which borders the Miocene Northern Apennines outcropping fold-and-thrust belt. Along with the PTF westernmost segment, a relevant Late Quaternary fault-scarp, known as Stradella thrust, extending for an overall length of 35–40 km, is outlined in the literature (Benedetti et al., 2003) and considered a debated seismogenic source of the DISS national database (DISS Working Group, 2021).

The instrumental seismicity is mainly concentrated at two distinct hypocentral ranges within the upper and the lower crust (Vannoli et al., 2015; Turrini et al., 2015), the latter extending mainly in the volume beneath the PTF domain.

No detailed geometric/kinematic and earthquake/fault association reconstruction is available for the Stradella thrust and the Emilia Arc. This paper is aimed to offer an update on the analysis of the seismogenic role of the emergent Stradella structure and to investigate its relationships with the buried Emilia Arc through a 3D seismotectonic reconstruction of the overall system that takes into account also new surface/shallow data.

We propose a multi-scale and multidisciplinary approach by combining local-scale morphotectonic (high-detailed GPS profiles, LiDAR images, and Unmanned Aerial Vehicles images) and geoelectric (Electrical Resistivity Tomography profiles, ERT) data, acquired on a key segment of the Stradella Thrust (Fig. 2), with the spatial-kinematic analysis of the seismicity occurred in a large study area centered on the Emilia Arc. Moreover, with a 3D methodological approach, we reconstruct the geometric-kinematic features of the Emilia Arc major thrusts and discuss their control on earthquake activity. For such purposes, we merged geological and geophysical data from the literature with new geological and seismological data. A digital model of major nonplanar fault surfaces was built, from near surface up to about 30 km deep. Original seismotectonic zoning was derived from the map-view projection of the seismogenic segments of the newly built 3D fault surfaces.

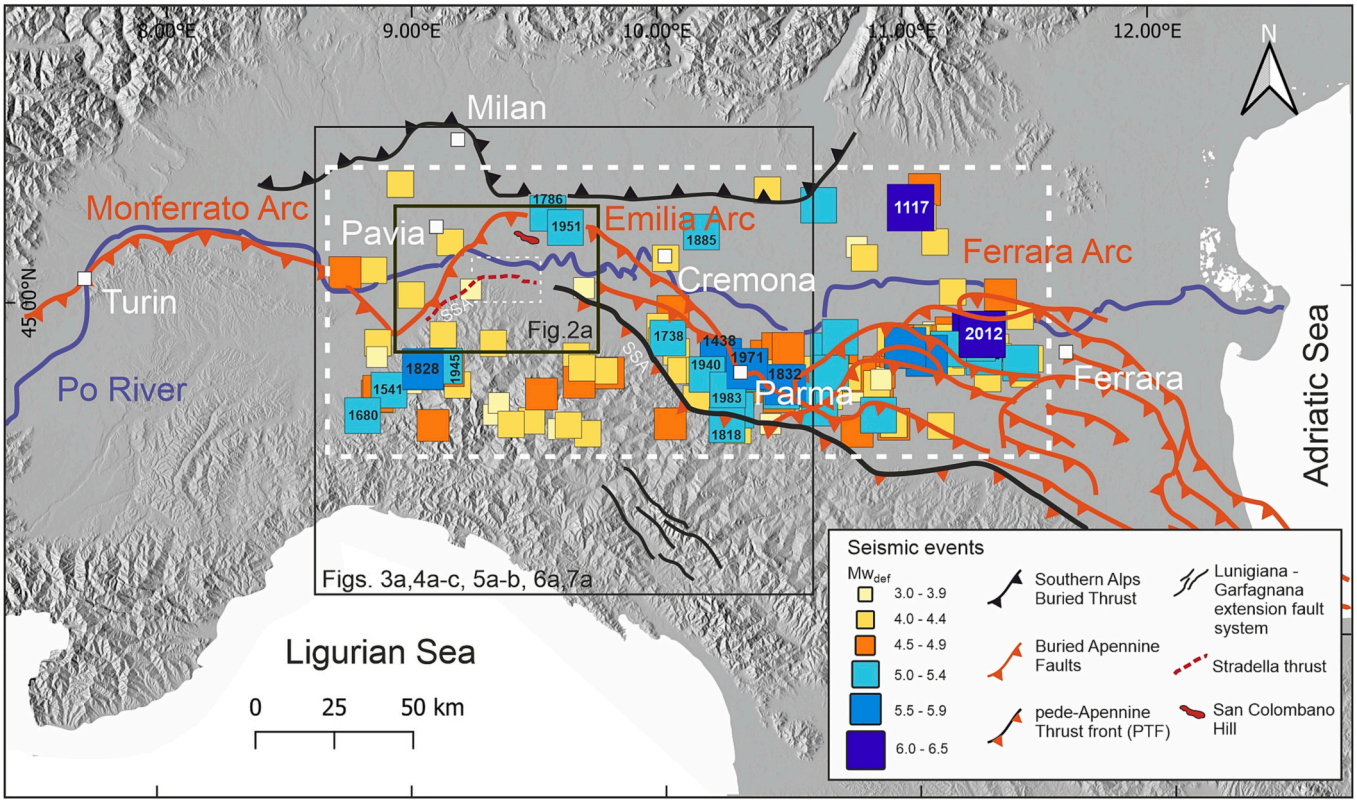

Fig. 1. Location map of the Stradella thrust and Emilia Arc in the Pliocene-Quaternary tectonic framework of northern Italy (after Benedetti et al., 2003). The smallest black and dashed white boxes show the location of Fig. 2a and b, respectively; the large black box shows the location of Figs. 3a, 4a,c, 5a,b, 6a, and 7a. Epicenters within the dotted white rectangle from 1000 CE to 2020 are from CPTI15 v.4 (Rovida et al., 2022); SSA stays for Stradella-Salsomaggiore Arc.

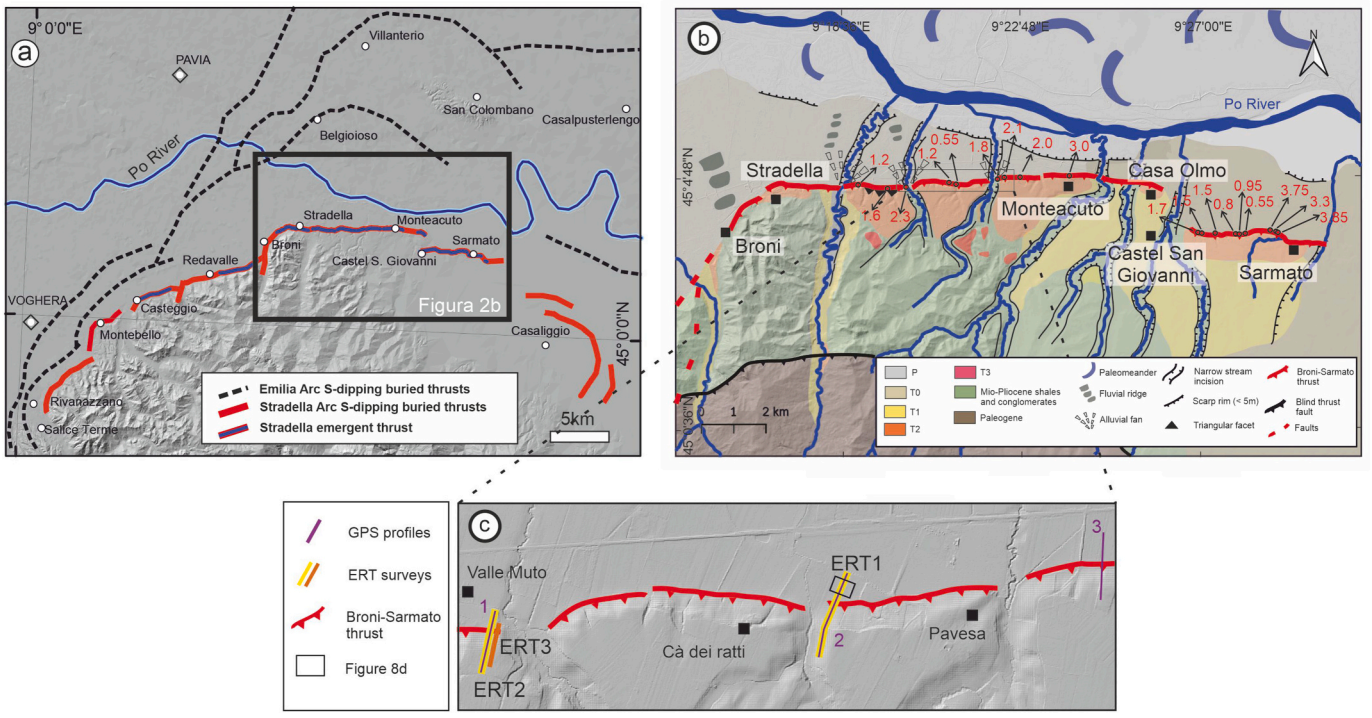

Fig. 2. Tectonic context and morphotectonic features of the Stradella-Salsomaggiore Arc. a) Fault trace of the Stradella thrust (from Rivanazzano to Sarmato) and of other structures of the Stradella-Salsomaggiore Arc as proposed in the present paper (see Fig.6), based on a critical review of available maps (e.g. Bigi et al., 1990; Martelli et al., 2017; CARG, 2016, Voghera sheet n.178); the black rectangle indicates the focus area including the Broni-Sarmato segment of the Stradella thrust. b) Geological and geomorphological map of the study area (small white rectangle in Fig. 1 and black rectangle in Fig. 2a), simplified from Benedetti et al. (2003), Pellegrini and Vercesi (1995) and original observations. Colours emphasize Paleogene, Miocene-Pliocene and Quaternary deposits. The area is characterized by fluvial terraces (T1, T2, T3) distinguishable by their elevation and weathering degree. T0 represents the coalescence surface of Apennines rivers deposits. Apennines rivers present strong erosional activity south of the Broni-Sarmato scarp, creating alluvial fans and fluvial ridges north of it. Triangular facets identified from the analysis of LiDAR (http://www.pcn.minambiente.it/mattm/progetto-pst-dati-lidar/) data are reported. The heights of the minor scarp (red numbers, in meters) of the Broni-Sarmato structure are reported. DTM layer is from Geoportale Regionale Regione Lombardia (https://www.geoportale.regione.lombardia.it/) and Geoportale Regionale Regione Emilia-Romagna (https://geoportale.regione.emilia-romagna.it/) both with a resolution of 5 m/pix. c) Location of high-precision GPS profiles (purple lines), ERT surveys (yellow and orange lines), and 3D model reconstructed from Unmanned Aerial Vehicles surveys (black square). (For interpretation of the references to colour in this figure legend, the reader is referred to the web version of this article.)

2. Geological background

2.1. Regional structures

The Apennines fold-and-thrust system of Northern Italy results from a northeastward migrating collisional process active since the Miocene and articulated in major well-distinct tectonic pulses and phases (Barchi and Beltrando, 2010). The latest one is late Pliocene-Quaternary in age and is involved in the deformation of the sedimentary deposits of the Pliocene-Quaternary foredeep (Pieri and Groppi, 1981; Castellarin and Vai, 1986; Bigi et al., 1990). The corresponding compressional belt is formed by four major structural arcs, the Monferrato Arc, the Emilia Arc, the Ferrara Arc (Fig. 1), and the Adriatic Arc . These arcs show younger ages of activity onset (see Ghielmi et al., 2013; Maesano et al., 2015) and progressively increasing amounts of shortening from west to east.

During the last 1.81 Ma, the cumulative slip-rate was ~0.70 mm/yr for the Emilia Arc, ~0.95 mm/yr for the Ferrara Arc, and up to ~1.40 mm/yr in the Adriatic Arc (Maesano et al., 2015). Such eastward increase is coherent with the counterclockwise rotation of the Northern Apennines during their emplacement (Bally et al., 1986; Cibin et al., 2003; Boccaletti et al., 2011; Carminati and Doglioni, 2012) and well matches the GPS observations (Devoti et al., 2011; Michetti et al., 2012). These data show a clear increase of the shortening across the Northern Apennines fronts passing from a low value (about 0.5 mm/yr), calculated along the Emilia Arc, to a higher one (about 2.4 mm/yr) calculated across the Ferrara Arc.

All arcs display strong asymmetry with shorter western limbs and more extended, smoother eastern ones (Cassano et al., 1986; Castellarin and Vai, 1986). This configuration is attributed to the presence within the Adria foreland of pre-existing Mesozoic tectonic discontinuities. The latter affected the subsequent foredeep basin infilling and controlled the progressive advance of the Apennine thrust front, leading to the present-day setting characterized by re-entrants separating the Northern Apennines arcs (Livani et al., 2018; Amadori et al., 2019).

Along with the Emilia Arc, the NNE-striking Pavia lateral ramp drove the NNE migration of the late.

Miocene to Quaternary Apennine contractional structures, whose outermost north-verging front is now located a few kilometers southward from the south-verging Alpine front (Gobetti and Perotti, 1990; Perotti and Vercesi, 1992; Benedetti et al., 2003; Toscani et al., 2006; Boccaletti et al., 2011; Michetti et al., 2012; Ghielmi et al., 2013; Vercesi et al., 2015; Maesano et al., 2015; Zuffetti et al., 2018a, 2018b) (Fig.1).

In fact, since the Late Miocene, the Po Plain foredeep was progressively reduced by the advance of the two opposite vergence belts (Fantoni and Franciosi, 2010; Toscani et al., 2014).

In a more internal position is located the Pede-Apennine thrust front (PTF), which runs along the southern margin of the Po-Plain and morphologically separates the outcropping foothills of the Apennines Mountain chain from the buried sector of the belt. The PTF also tectonically separates an internal Apennine domain, having the onset of the deformation in late Messinian-early Pliocene, with an external domain mainly deforming during Late Pliocene and Quaternary (Pieri and Groppi, 1981). Drainage anomalies and isolated reliefs highlight deformation in the last 1.8 Ma of both the PTF and Emilia Arc (Burrato

et al., 2003; Galli, 2005; Toscani et al., 2006; Maesano et al., 2015). The PTF, located in the rear of the Emilia Arc, is characterized by a northward convex arcuate shape, in this paper referred to as Stradella-Salsomaggiore Arc (SSA in Fig. 1). The western and central sector of such an arc, known in the literature as Stradella thrust, shows a relevant Late Quaternary fault-scarp for an overall length of about 40 km (Benedetti et al., 2003).

The uplift of the Stradella structure, along the northern termination of the Emilia PTF, was active at least since Late Pleistocene times and caused the outcropping of Messinian calcarenites within the Po River bed (Tellini et al., 2001).

An ongoing, although buried, fold-and-thrust activity in the Late Pleistocene of the Emilia Arc is revealed by the San Colombano Structure (Zuffetti and Bersezio, 2020; Figs. 1 and 2a). The Colombano hill represents an anticline hinge zone and coincides with a change in the direction of the Emilia Arc; the arc is characterized by a NE-SW trend within the Po Valley up to San Colombano, where it switches to an NW-SE direction.

Active shortening along the Emilia Arc and, possibly, the Pede-Apennines system in correspondence with the Stradella thrust, is indicated by the presence of moderate seismicity, whose focal mechanism solutions indicate compression (Gasparini et al., 1985; Boccaletti et al., 1985; Anderson and Jackson, 1987; Pondrelli et al., 2006, 2011; Lavecchia et al., 2015; Boncio and Bracone, 2009; Ciaccio et al., 2021; Peruzza et al., 2021) and by GPS measurements (Serpelloni et al., 2005, 2007; D'Anastasio et al., 2006; Cenni et al., 2008; Devoti et al., 2011; Bennett et al., 2012). Furthermore, active stress data and studies on breakout boreholes show a good match between the mean NNW-SSE striking maximum horizontal stress and the WNW-ESE direction of the Emilia Arc frontal thrust direction's (Carafa and Barba, 2013; Montone and Mariucci, 1999; Montone et al., 2012).

The instrumental seismicity highlights a prevalence of activity at lower crustal depths (Vannoli et al., 2015; Turrini et al., 2015), making, however difficult its association with the near surface structures.

2.2. Previous morphotectonic studies on Stradella thrust

The Stradella thrust, first outlined by Benedetti et al. (2003), is a late Quaternary south-dipping emerging thrust locally associated with a clear morphotectonic feature. It extends in the WSW-ENE direction from Rivanazzano to Broni and in the E-W direction from Broni to Sarmato, for a total length of about 40 km (Fig. 2a).

Geological, geomorphological, and hydrographical features indicate recent tectonic activity, especially clear for Broni-Sarmato segment (Fig. 2b). This segment is associated with a morphotectonic scarp that extends for ~14 km in the WSW-ENE direction from Montebello to Broni, about 13 km in the E-W direction east of Broni, and another ~4 km from Castel San Giovanni to Sarmato in the E-W direction (Pellegrini and Vercesi, 1995; Benedetti et al., 2003) (Fig. 2b). According to Benedetti et al. (2003), the fault scarp shows cumulative surface throws of 2 to 25 m. Based on the scarp degradation analysis, the same authors suggest a minimum uplift rate of 0.3 mm/yr in a time interval of 35 ka. Furthermore, they attribute the activity to a N-S to N°15 W direction of shortening, which would determine prevailing dip-slip kinematics on the E-W segments and a relevant left-lateral component on WSW-ENE segments.

The Broni-Sarmato topographic high identifies a topographic-structural obstacle that precluded the deposition of Pliocene marine sequences and Pleistocene continental deposits (Pellegrini and Vercesi, 1995). Alluvial terraces of Quaternary age are mainly developed between Stradella and Castel San Giovanni (Pellegrini and Vercesi, 1995) (Fig. 2b).

Benedetti et al. (2003) showed that Apennines tributaries of the Po River generated terraces T1, T2 and T3 (Fig. 2b) due to the continuous uplift of the area during Middle Pleistocene (terraces T2 and T3) and the latest Pleistocene (T1). The thrust escarpment delimits to the north terraces T1 and T2 and bounds to the south the T0 surface resulting from the coalescence of the Apennines rivers deposits.

3. Methods and techniques

3.1. Geomorphological survey

We investigated in the field the Broni-Sarmato segment of the Stradella thrust for a total length of 18 km (Fig. 2b). In order to better define the geometry of the associated scarp previously investigated by Benedetti et al. (2003) and to select the best site for geoelectric surveys, we carried out a new detailed geomorphological analysis using high-resolution remotely-sensed images and aerial photos. This allowed us to identify and map the morphostructures characterizing the investigated area. Aerial photographs at 1:20,000 scale were acquired by the General Aerial Photography Company in 1980. Each photo overlaps 60% along the acquisition direction and 25% in the transversal direction with the other photos. Morphostructures have thus been mapped using stereoscopic techniques.

To obtain a more precise depiction of the scarp and to evaluate the variation of the vertical displacement, 31 perpendicular-to-fault morphological profiles were carried out using a DTM derived from LiDAR data available on the Italian National Geoportal (http://www.pcn.minambiente.it/mattm/progetto-pst-dati-lidar/), relative to the Lombard portion of the fault from Broni to Monteacuto (Fig. 2b). Data are characterized by an altimetric accuracy of 15 cm and a planimetric accuracy of 30 cm. These LiDAR profiles were thus focused on a more localized 11 km-long segment with respect to the analysis carried out by Benedetti et al. (2003), who considered 12 GPS profiles for the whole length of the Stradella thrust.

Due to the extent of the fault and its proximity to several urbanized areas, it has been possible to survey by an Unmanned Aerial Vehicle (UAV) only very limited portions of the scarp. The used UAV is a quadricopter DJI Spark equipped with a 12 Megapixel stabilized camera, an integrated GPS satellite positioning system, and a flying autonomy of 16 min without wind. The UAV captured images every 2 s during a constant velocity flight of 3 m/s at an altitude of 30 m using the Structure from Motion (SfM) technique. Each acquired photo is characterized by lateral and vertical overlap of 90% with the others. Using the procedure suggested in the literature (Bonali et al., 2019), these images have been processed with the aid of Agisoft Photoscan to create DTM (Digital Terrain Model), DSM (Digital Surface Model), and shaded models for the study areas.

The scarps were also studied by high-resolution GPS surveys, capable of achieving centimeter precision. All data were acquired at a distance of 5 m from the others, maintaining a fixed position for two minutes each, to minimize the position error and increase data accuracy; measure points were positioned along an ideal straight line. The collected data have been subsequently corrected, taking the stationary position of the base station PAVI as reference: this correction is needed because the base-GPS distance was >15 km for all the analyses time (Takasu and Yasuda, 2009).

3.2. Geoelectrical surveys

Three Electrical Resistivity Tomography (ERT) profiles with NNE-SSW orientation and different lengths were acquired at two selected test sites (location in Fig. 2c) located on the fault-scarp section between Broni and Pavesa, which is especially well evident and marked by triangular facets. The ERTs were located roughly orthogonal to the thrust scarp. A 470 m long (ERT1) and a 329 m long (ERT2) profiles provided great depth of investigation (down to approximately 70 and 50 m, respectively). A shorter profile (ERT3, 94 m long) provided high accuracy at shallow depths (approximately 15 m). Profiles ERT2 and ERT3 were acquired on 21st September 2020, and profile ERT1was acquired on 28th January 2021 (for locations, see Fig. 2c). The profiles

were obtained using 48 electrodes spaced 10, 7 and 2 m apart, respectively, in profiles ERT1, ERT2, and ERT3.

Each profile was collected using 306 Wenner-Schlumberger array quadrupoles which ensure high vertical resolution and signal amplitude, and 328 dipole-dipole array quadrupoles, which provide enhanced lateral resolution. A fully automatic multi-electrode resistivity meter SYSCAL Jr. Switch-48 by IRIS Instruments was used for data collection.

Data inversion was performed using ERTLab Solver (Release 1.3.1, by Geostudi Astier s.r.l. - Multi-Phase Technologies LLC), based on tetrahedral Finite Element Modelling (FEM). Tetrahedral discretization was used in both forward and inverse modelling. The foreground region was discretized using a 5 m cell size for profile ERT1, a 3.5 m cell size for profile ERT2 and a 1 m cell size for profile ERT3, i.e., half the electrode spacing, to give the model higher accuracy. The background region was discretized using an increasing element size towards the outside of the domain, according to the sequence: 1×, 1×, 2×, 4× and 8× the foreground element size.

The forward modelling was performed using mixed boundary conditions (Dirichlet-Neumann) and a tolerance (stop criterion) of 1.0E-7 for a Symmetric Successive Over-Relaxation Conjugate Gradient (SSORCG) iterative solver. Data inversion was based on a least-squares smoothness-constrained approach (LaBrecque et al., 1996). The noise was appropriately managed using a data-weighting algorithm (Morelli and LaBrecque, 1996) that allows the adaptive changes of the variance matrix after each iteration for those data points the model poorly fits. The inverse modelling was performed using a maximum number of internal inverse Preconditioned Conjugate Gradient (PCG) iterations of 5 and a tolerance (stop criterion) for inverse PCG iterations of 0.001. The amount of roughness from one iteration to the next was controlled to assess maximum layering: a low value of reweight constant (0.1) was set to generate maximum heterogeneity.

The resistivity models were obtained by merging and jointly inverting datasets from different arrays, which can deliver better detectability and imaging and, hence, provide more accurate models (Szalai et al., 2009; Torrese, 2020) and more reliable ERT imaging (DelaVega et al., 2003). Inversion involved the application of homogeneous starting models that set the average apparent resistivity value at each node. The final inverse resistivity models were chosen based on the minimum data residual (or misfit error).

3.3. Seismicity analysis

We aim to define the active deformation field and the seismotectonic context of the Stradella Thrust in the Emilia Arc and the more internal Stradella-Salsomaggiore Arc frame (Figs. 1, 3, 4, and 5). In order to contribute to constraining the active deformation field and the depth geometry of the involved tectonic structures, we analyzed the instrumental seismicity that occurred between 1985 and 2020 (Fig. 3a), recorded by the National Seismic Network (RSN) and the Regional Seismic network of North-western Italy (RSNI) (Fig. S1). We used data from the Italian Seismic Bulletin (ISB) spanning from 1985 to 2020 (ISIDe Working Group, 2007), also considering the RSNI bulletin (1990–2018) and the events falling in our study area relocated by Peruzza et al. (2021). The dataset includes nearly 3500 earthquakes with $0.4 \leq M_L \leq 4.9$ (Fig. 3a and b).

We followed a multi-step analysis that consists of: 1) general characterization of seismicity; 2) spatial analysis; 3) focal mechanism compilation from literature and computation of new ones; 4) kinematic analysis.

1) We first described the seismic activity in terms of daily seismicity rates, cumulative number of earthquakes, and cumulative moment release (Figs. 3c, d). Then, the statistical analysis was performed using the ISB without filtering the seismic catalog to avoid losing information. We computed the parameters of the frequency–magnitude relationship on the Gutenberg and Richter (1956) model (GR) and the completeness magnitude (Mc) (Fig. 3e); we estimated Mc using the best combination of Mc95, Mc90, and Maximum Curvature (Woessner and Wiemer, 2005) and its uncertainty with the bootstrap technique (Wiemer and Wyss, 2000). We defined the GR parameters applying the maximum likelihood method (Aki, 1965; Utsu, 1965) using ZMAP software (Wiemer, 2001).

2) We identified spatial seismicity clusters by using the Kernel Density Estimation (KDE), which is a common approach for exploring spatial point patterns in geospatial analysis (Brunsdon, 1995; Baddeley et al., 2015; Zhang, 2022). The clusters were detected by applying the ArcGis processing tool that calculates the density in a circular neighbourhood around each seismic event considering the kernel function proposed in Silverman (1986). The final map was obtained by setting the search radius to 8 km (Fig. 4a). For each selected cluster, we examined the depth distribution and the energy release (ER) (Fig. 4b and c).

We analyzed the depth distribution of events by using histograms and the probability density function (pdf) computed via non-parametric density estimation (KDE) with a gaussian kernel function and a bandwidth value of 2. The histograms are plotted with a bin of 1 km only to show the distribution of the dataset underlying the pdf function (Fig. 4b). Finally, we computed ER applying the magnitude – energy relationship ($\log E = 9.4 + 2.14M_L + 0.054M_L^2$, Richter, 1958) valid for $M_L \leq 4.5$ (Fig. 4c) (Okal, 2019) only to highlight the areas with higher magnitudes.

3) We collected the focal mechanisms solutions (FMs) available in the study area from RCMT, TDMT, and detailed papers (Frepoli and Amato, 1997; Montone and Mariucci, 2016; Scognamiglio et al., 2006; Eva et al., 2014; Pondrelli et al., 2020), and we detected the most energetic events, belonging to the selected clusters, to compute other focal mechanism solutions (Fig. 5a and S2). To this aim, we considered the waveforms of the selected events recorded by the RSN and RSNI. We gathered an amount of 1888 three-component recordings that were analyzed by visual inspection considering only the waveforms associated with the seismic stations falling within a ray of 130 km by the centroid of the study area (Fig. S1). The P polarities are inverted by using the FPFIT standard procedure (Reasenberg and Oppenheimer, 1985). We selected the solutions from this data set with a minimum number of eight clear observations homogeneously distributed on the focal sphere and with less than two discrepant polarities. The selection was further checked based on the two quality factors (Q) of the FPFIT code, decreasing from A to C; these are the degree of polarity misfit (Qf) and the range of uncertainties of the strike, dip, and rake (Qp) in a solution, respectively. The new focal mechanisms parameters (details in Table S1 and Fig. S2) and the collected focal mechanism solutions from the literature are listed in Table 1.

4) We computed the P, T, and B axes of the FMs and performed a kinematic classification applying the criteria of Zoback (1992) (Fig. 5b). Finally, we concluded the kinematic analysis by computing, when possible, the average focal mechanism (AFM) for each cluster. The AFMs were evaluated by applying the Bingham statistical procedure (Allmendinger et al., 2012) used to describe axial data on a sphere. This approach, applicable when there are no large differences in magnitude, allows finding the best-fit axes (the common extension, intermediate and shortening axes) of an ensemble of FMs and consequently to define the representative one (AFM).

3.4. Fault alignments identification and 3D-fault model building

To build a 3D-geometric fault model of the Stradella thrust, of the overall Stradella-Salsomaggiore Arc and the Emilia Arc thrust systems, as depicted in Fig. 6, we integrated geological and seismological data following the methodological approach of the Community Fault Model of Southern California (Nicholson et al., 2014; Plesch et al., 2007). In particular, we adapted to a buried thrust context, the procedure recently applied to the intra-Apennines extensional faults (Lavecchia et al., 2017; Castaldo et al., 2018; Bello et al., 2021; Cirillo et al., 2021).

Without continuous seismicity patterns extending from the surface to the base of the seismogenic layer, the fault geometry at depth

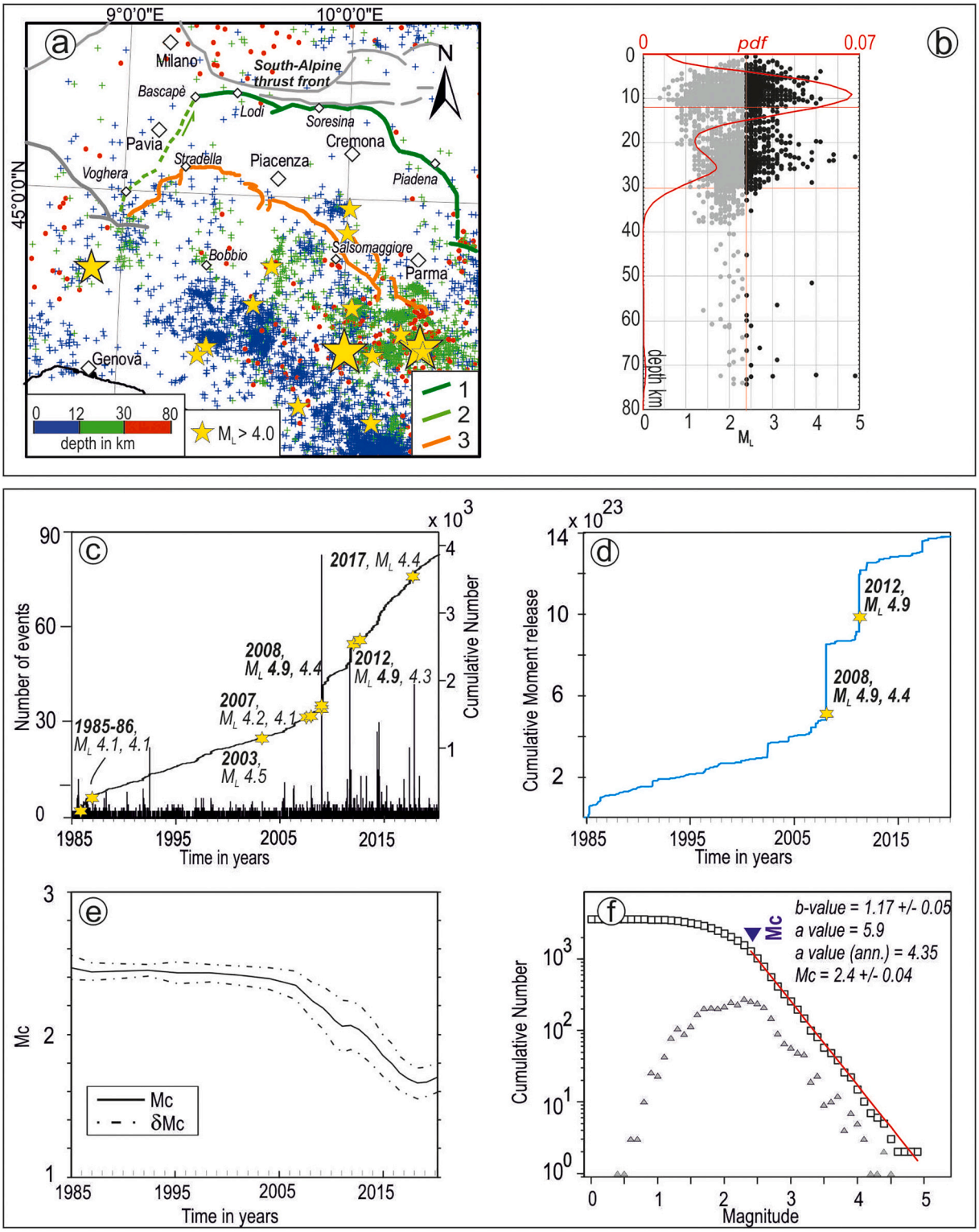

Fig. 3. Characterization of the instrumental seismicity in the study area (see location in Fig. 1) and neighboring regions. a) Epicentral distribution of earthquakes from the Italian Seismic Bulletin occurred between 0 and 74 km in the period 1985–2020 (0.4 ≤ ML ≤ 4.9). The depicted geological structures are: 1- north-verging buried thrust front of the Emilia Arc, 2- lateral transfer fault of the Emilia Arc; 3- Pede-Apennine thrust front along the Stradella-Salsomagiore Arc. b) depth distribution of the seismicity represented as probability density function (pdf, red line) and in terms of magnitude. The black dots represent the events, over the completeness magnitude, considered for the pdf calculation. C) Daily and cumulative number of events. The yellow stars represent earthquakes with ML >4.0. d) Cumulative moment release; yellow stars are the most energetic events that highlight the greatest seismic moment releases. E) Completeness magnitude vs. time. F) Gutenberg–Richter slope evaluated with the 3500 events represented in panels a); in blue, the completeness magnitude Mc. (For interpretation of the references to colour in this figure legend, the reader is referred to the web version of this article.)

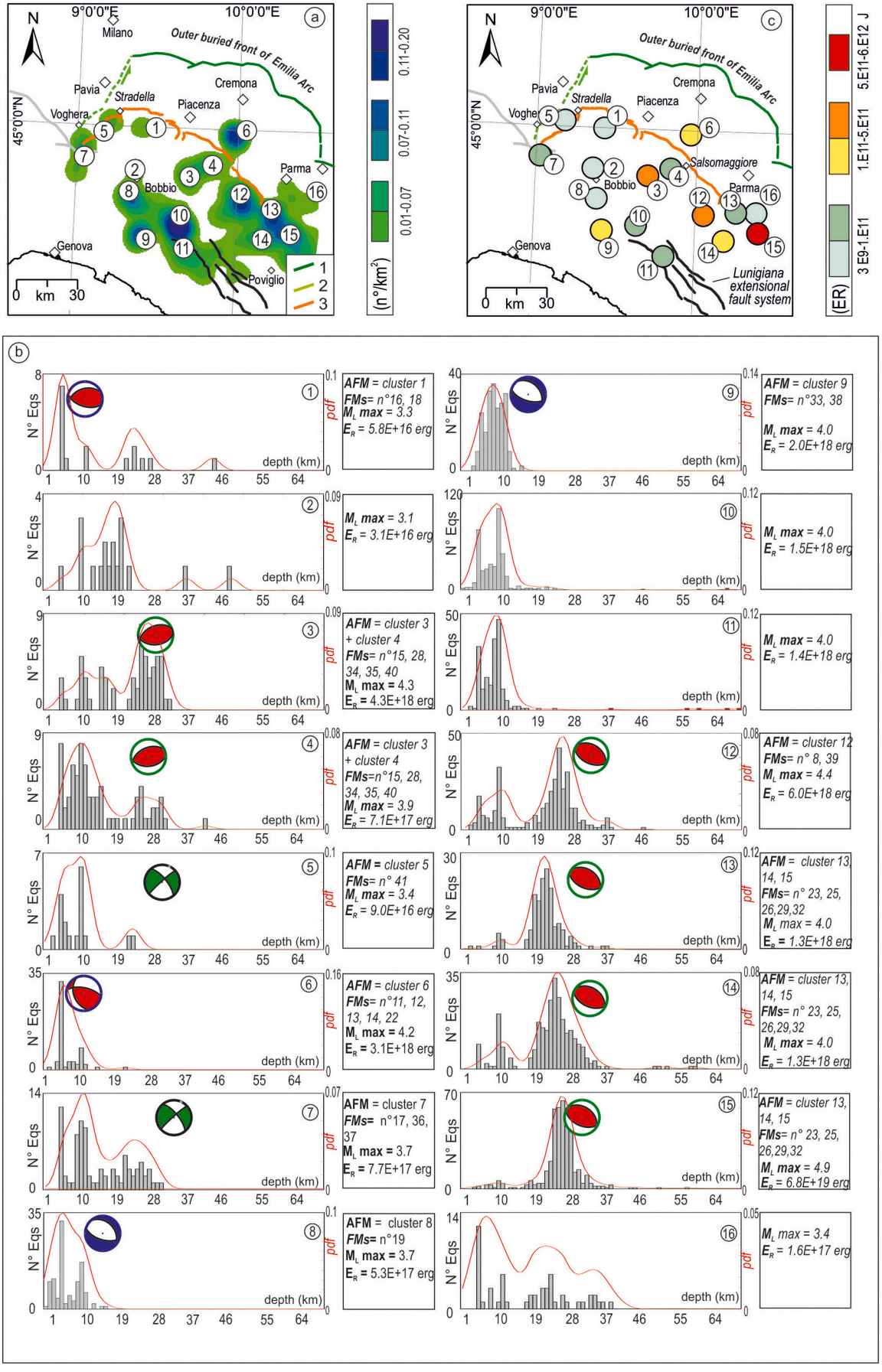

(caption on next page)

Fig. 4. Geospatial earthquakes analysis. A) Map of the seismicity clusters (1–16) detected by the Kernel Density Estimation computed using the data of the Italian Seismic Bulletin (time period 1985–2020; 0.4 ≤ ML ≤ 4.9; depth 0–74 km); fault key as in Figure3. b) Depth earthquake distribution of the clusters 1–16 represented as histograms and as probability density function (pdf, red line). The focal mechanisms plotted in the panels are the Average Focal Mechanisms (AFM) representing the kinematics of each cluster. The position and the border colour of AFM represents the depth association following the colour code as in Fig. 3a). Seismicity clusters and Focal Mechanisms (FMs) used in the AFMs calculation are specified on the right side of each panel, together with Maximum Magnitude (M_L max) and Energy Release (ER). C) Map of the energy released (ER) by each selected cluster. (For interpretation of the references to colour in this figure legend, the reader is referred to the web version of this article.)

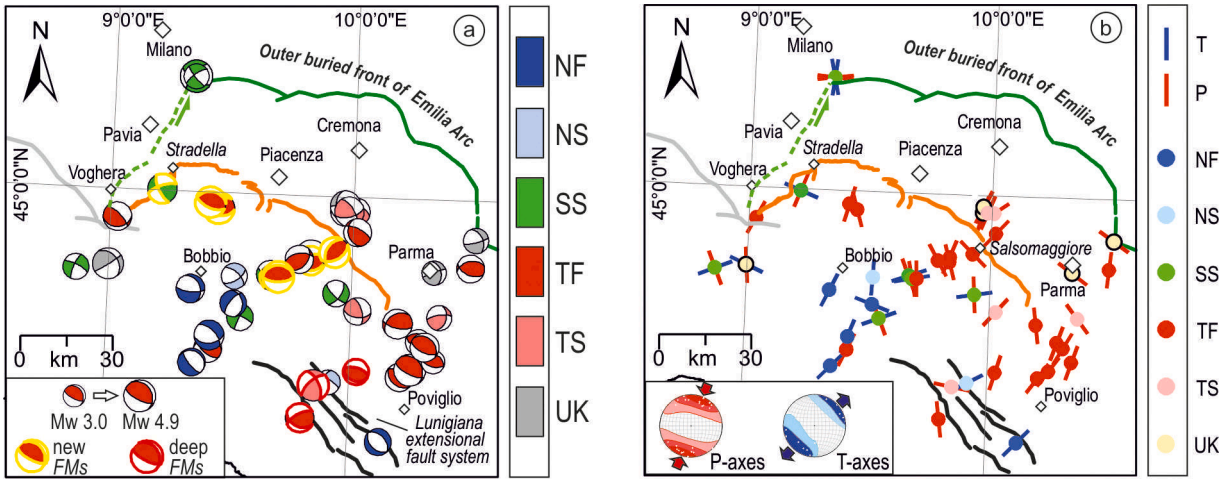

Fig. 5. Focal mechanism and P, T axes. A) Map of the calculated (yellow colored border) and compiled focal mechanisms (FMs) reported in Table 1, fault key as in Figure3. The FMs colour refers to the Zoback kinematic classification (NF = Normal fault, NS = Normal oblique fault, SS = Strike Slip fault, TF = Inverse fault, TS = Inverse oblique fault, UK unknown solution). B) Map of the P and T axis distribution of FM solutions; the left lower inset represents the average axes of the reverse/reverse oblique and normal/normal oblique FMs, respectively. (For interpretation of the references to colour in this figure legend, the reader is referred to the web version of this article.)

exclusively derived from seismological data can be ambiguous, and various solutions can be obtained. To better constrain the deep geometry, we connected the shallow-depth fault surfaces derivedfrom geological data with the clusters of seismicity favouring geometries that interpolate (a) the maximum density of earthquakes, (b) the maximum magnitude events and (c) homogeneous kinematic hypocentral volumes.

The procedure is articulated in five steps:

Step 1 – In the first step, we collected and organized, on a GIS platform, the available multi-scale geological information across the study area, also redrawing part of it. Specifically, we compiled a georeferenced raster database of geological structural maps and sections: Sheets of Geological Map of Italy at scale of 1:100,000; Structural Model of Italy at scale of 1:500,000 (Bigi et al., 1990); regional geological and seismotectonic maps at scale of 1:250,000 (Martelli et al., 2017); structural maps from selected papers (Pieri and Groppi, 1981; Cassano et al., 1986; Fantoni and Franciosi, 2010; Boccaletti et al., 2011); geological transects from Pieri and Groppi (1981) and many other papers reported in Figs. S3 and S4. Subsequently, we created new shape files redrawing: a) the traces of the collected cross-section and transects (Fig. S3 with references); b) the depth contour lines of the Pliocene deformed foredeep domain derived from the Structural Model of Italy (scale 1:500,000) with associated anticline and syncline hinges and major thrust structures (Fig. 6a). Integrating the above information, we identified and drew the buried traces of first-order master fault alignments which delimited well distinguished kinematic blocks with a northward rejuvenating age in the offset phase (Fig. 6b). The along-strike segmentation of these alignments was defined considering both sharp variation in trend, axial culmination, depression, as well as the length of the hanging-wall anticlines.

Step 2 - After importing the described data on the MOVE 3d platform (MOVE suite software by PetEx Ltd., version 2019.1), we built the 3D shallow fault surfaces of the identified fault alignments by extruding them to depths of a few kilometers (4–5 km) after deriving the dip angle from the collected geological cross-sections and regional transects.

Step 3 - The seismicity was suitably filtered (RMS ≤ 0.5 s, gap ≤180, phase readings N > 10, vertical error ≤ 4 km; horizontal error ≤ 3 km) and then projected along the geological sections of Figs. S3 and serial closely spaced transects (Fig. S5) perpendicular to the structural trends assuming a variable half-width (5 and 10 km). Next, using the MOVE software section view tool, we draw the fault traces connecting the shallow fault surfaces with the hypocentral volumes corresponding to the seismicity clusters and the background seismicity.

Along the traces of four regional transects (sec 0, 1, 2, and 3 in Figs. 7 and S5), corresponding to interpreted seismic lines (Pieri and Groppi, 1981) (Fig. S4), we also adopted a section-view density contour representation of identified hypocentral clusters lying within semi-widths between 15 and 25 km from the fault traces (Figs. 7 and S5); the density contours were obtained applying the Kernel Density Estimation (KDE) in geospatial analysis (Brunsdon, 1995). Such a representationhighlights the areas with the highest number of earthquakes, sometimes hidden by the diffuse background seismicity, and is helpful in better correlating the seismicity with the surface position of the thrust system. Along the four transects, we also projected the focal mechanisms of events after the 2000s, whenever sufficiently well constrained at depth (Table 1).

Step 4 - Using the Delaunay triangulation method (Delaunay, 1934; Okabe et al., 1992) of the MOVE suite, we interpolated in a 3D space the map and section view traces of the fault alignments to build nonplanar fault surfaces down to the base of the seismogenic layer. From the 3D fault models, we extracted two km-spaced smoothed depth contour lines of each fault surface.

Step 5 – In the final step, we performed a validation and reliability evaluation of the reconstructed 3D geometries considering that it depends on 1) the spatial uncertainty of the position of the buried fault alignment and their shallow depth extrapolation, 2) the earthquake distribution (seismic gaps, diffuse or clustered events) and the formal errors of seismic locations.

Table 1
Summary of the source parameters of the focal mechanisms computed in this study and available in the literature.

Date	time	Long	Lat	depth	ML/Md	Mw	Strike	Dip	Rake	P_tr	P_pl	T_tr	T_pl	Kin	Ref-(ID)
15/05/1951	22.54.28	9.33	45.33	6.0	–	5.0	235	73	−171	98	18	190	6	SS	1-(1)
16/05/1951	02.27.01	9.33	45.33	6.0	–	4.5	123	64	−17	84	30	350	7	SS	1-(2)
15/07/1971	01.33.22	10.34	44.78	8.0	–	5.3	346	42	8	308	26	196	36	UK	2-(3)
25/10/1972	21.56.13	9.92	44.45	40.0	–	5.2	195	51	−24	165	41	63	11	NS	2-(4)
15/04/1974	21.49.00	9.55	44.63	5.0	–	4.6	296	81	−175	160	8	251	2	SS	2-(5)
16/11/1975	13.04.00	9.52	44.75	20.0	–	4.8	312	62	−32	275	42	185	0	NS	1-(6)
22/08/1976	02.49.00	9.52	44.67	8.0	–	4.6	351	32	−133	166	60	292	18	NF	2-(7)
23/12/1980	12:01:03	9.94	44.71	10.0	–	4.6	35	61	−20	358	34	263	8	SS	1-(8)
09/11/1983	16:29:51	10.36	44.64	28.1	–	5.0	14	43	29	324	16	215	49	TS	1*-(9)
01/10/1986	19:53:41	10.13	44.27	23.6	4.1	4.5	135	43	−91	245	88	46	2	NF	1*-(10)
31/10/1991	09:31:18	10.01	44.95	4.5	4.0	–	180	70	140	237	11	137	42	TS	3-(11)
01/01/1992	10.12.19	9.96	44.95	3.3	3.4	–	150	35	150	19	22	139	51	UK	3-(12)
02/01/1992	13.44.59	9.96	44.96	1.3	3.4	–	170	40	170	28	28	143	38	UK	3-(13)
11/02/1995	4.22.26	9.98	44.95	7.6	3.1	–	75	60	30	23	3	290	41	TS	4*-(14)
14/06/1995	05.27.03	9.83	44.81	8.5	3.2	–	120	45	100	23	0	116	83	TF	4*-(15)
21/02/2002	10.33.12	9.44	44.90	14.6	3.1	–	235	50	60	346	1	78	67	TF	1 N-(16)
11/04/2003	09:26:58	8.86	44.75	8.2	4.5	4.8	297	75	−165	160	21	250	0	SS	1*-(17)
21/09/2004	10.51.05	9.41	44.96	11.7	3.3	–	115	60	100	198	14	50	73	TF	2 N-(18)
18/04/2005	10.59.18	9.34	44.70	30.2	3.7	4.0	336	34	−35	330	54	208	21	NF	1*-(19)
07/04/2006	14.01.16	9.86	44.43	8.5	3.3	–	335	60	30	283	3	190	41	TS	4*-(20)
09/05/2007	06:03:49	10.48	44.73	22.6	–	4.2	258	45	63	187	3	88	71	TF	1*-(21)
30/07/2007	19:05:43	10.02	44.80	27.8	–	…	297	67	66	45	19	171	61	TF	2*-(22)
31/12/2007	10.05.00	10.25	44.49	22.1	3.1	–	330	25	120	218	22	6	64	TF	4*-(23)
26/03/2008	09:19:30	9.81	44.34	72.2	–	4.0	243	66	61	354	16	112	58	TF	5-(24)
23/12/2008	21:58:25	10.34	44.51	24.6	–	5.5	295	34	97	200	11	0	78	TF	1*-(25)
23/12/2008	23.37.06	10.28	44.57	25.4	4.0	4.9	286	34	84	200	11	38	78	TF	1*-(26)
25/12/2008	03.08.29	10.31	44.56	26.1	3.9		115	60	80	212	14	0	73	TF	4*-(27)
19/10/2009	10.08.50	9.83	44.80	15.0	–	3.9	250	60	80	347	14	135	73	TF	3 N-(28)
08/09/2011	13.17.27	10.19	44.62	19.4	–	3.6	103	66	115	175	17	51	61	TF	5*-(29)
20/10/2011	06:11:18	9.42	44.53	6.6	4.0	4.2	278	34	62	208	14	78	69	TF	1*-(30)
25/01/2012	08.06.36	10.50	44.87	30.3	–	5	335	46	−16	306	39	198	21	UK	1*-(31)
27/01/2012	14.53.13	10.03	44.48	60.8	–	4.9	286	63	87	18	18	189	72	TF	2*-(32)
05/03/2012	15.15.06	9.35	44.48	20.6	–	44.3	297	19	−114	64	62	226	27	NF	1*-(33)
03/10/2012	14.41.29	9.66	44.75	21.3	–	4.5	25	80	−20	340	21	73	7	SS	4 N-(34)
03/10/2012	17.18.01	9.70	44.75	24.0	3.2	–	90	65	90	180	20	360	70	TF	5 N-(35)
19/10/2013	16.21.57	8.99	44.77	22.3	–	3.3	58	86	54	177	31	296	38	UK	4*-(36)
21/11/2013	10:36:49	9.02	44.91	5.4	–	4.0	86	27	44	30	24	253	59	TF	1*-(37)
30/11/2014	09.34.25	9.42	44.57	12.0	–	3.6	315	57	−58	280	63	23	7	NF	5*-(38)
19/11/2017	12.37.44	10.03	44.66	22.0	–	4.4	344	64	136	43	8	304	49	TS	5*-(39)
22/05/2019	14.37.36	9.92	44.82	18.0	3.5	–	60	50	110	136	3	35	74	TF	6 N-(40)
19/04/2020	09.53.41	9.20	44.99	28.0	3.7	–	252	71	21	23	1	114	28	SS	7 N-(41)

1 = Montone and Mariucci, 2016; 2 = Pondrelli et al., 2020; 3 = Frepoli and Amato, 1997; 4 = Eva et al., 2014; 5 = TDMT Scognamiglio et al., 2006; * = location from CSI/seismic bulletin; N = new focal mechanisms computed in this study). Key: P_tr = trend of P-axes, P_pl = plunge of P axes, T_tr = trend of T-axes, T_pl = plunge of T axes, kin = kinematic associated to each focal mechanism following Zoback (1992) classification (TF = thrust, TS = thrust-strike, SS = strike, NF = normal, NS = normal strike.

Since the near-surface fault traces are almost all buried, we evaluated the uncertainty on the alignment position considering the average spatial variations observed in different structural maps for the same structural element. Then, we considered the maximum vertical formal error of the dataset as depth uncertainty since the seismic events used to define the depth geometry were previously filtered. Finally, we considered the availability and quality of the geological and seismological input data and attributed to the major segments of each fault alignment a quality parameter per data typology defined as Constrained (C), Poor Constrained (PC), Extrapolated (E) (see Table S2).

The inner blue clusters represent upper crust extensional seismicity located along the northward buried prosecution of the Lunigiana fault system; the light-green clusters represent shallow-to-deep crustal seismicity associated with the high angle SE dipping Pavia left-lateral ramp; orange clusters are associated to the Stradella-Salsomaggiore Arc; the green, purple and violet ones are related to the outermost frontal thrust of the Emilia Arc and its hanging-wall splays, respectively; the pink cluster highlights a possible antithetic splay to the outermost thrust.

4. Results

4.1. Morphostructural data

Integrating the newly collected data, we reconstruct the surface geometry of the Broni-Sarmato fault-scarp in more detail than previously done.

i) The trace of the morphological feature extends 18 km along-strike in an average E-W direction, following the contact between the Miocene marls and the Quaternary sands and clays. The trace is not continuous, as previously reported in the literature (Benedetti et al., 2003). Indeed, it is characterized by one first-order right-stepping with a perpendicular-to-strike separation of 1.8 km between the villages of Casa Olmo and Castel San Giovanni (Fig. 2b) and by diffuse second-order left- and right-steps with a total of 4 segments. These have along-strike extent between 1.5 and 9 km with small separation gaps (perpendicular to strike) in the order of 60 to 260 m. The en-échelon steps show a gradual decrease of the scarp height at the tips of the onlapping segments. These segments exclude those that coincide with interruption of the fault scarp due to river erosion.

ii) A secondary scarp is located at the foot of the main one, parallel to it. It extends for 13.5 km in length, as can be seen from the points of measurements in Fig. 2b (red numbers). The second scarp does not

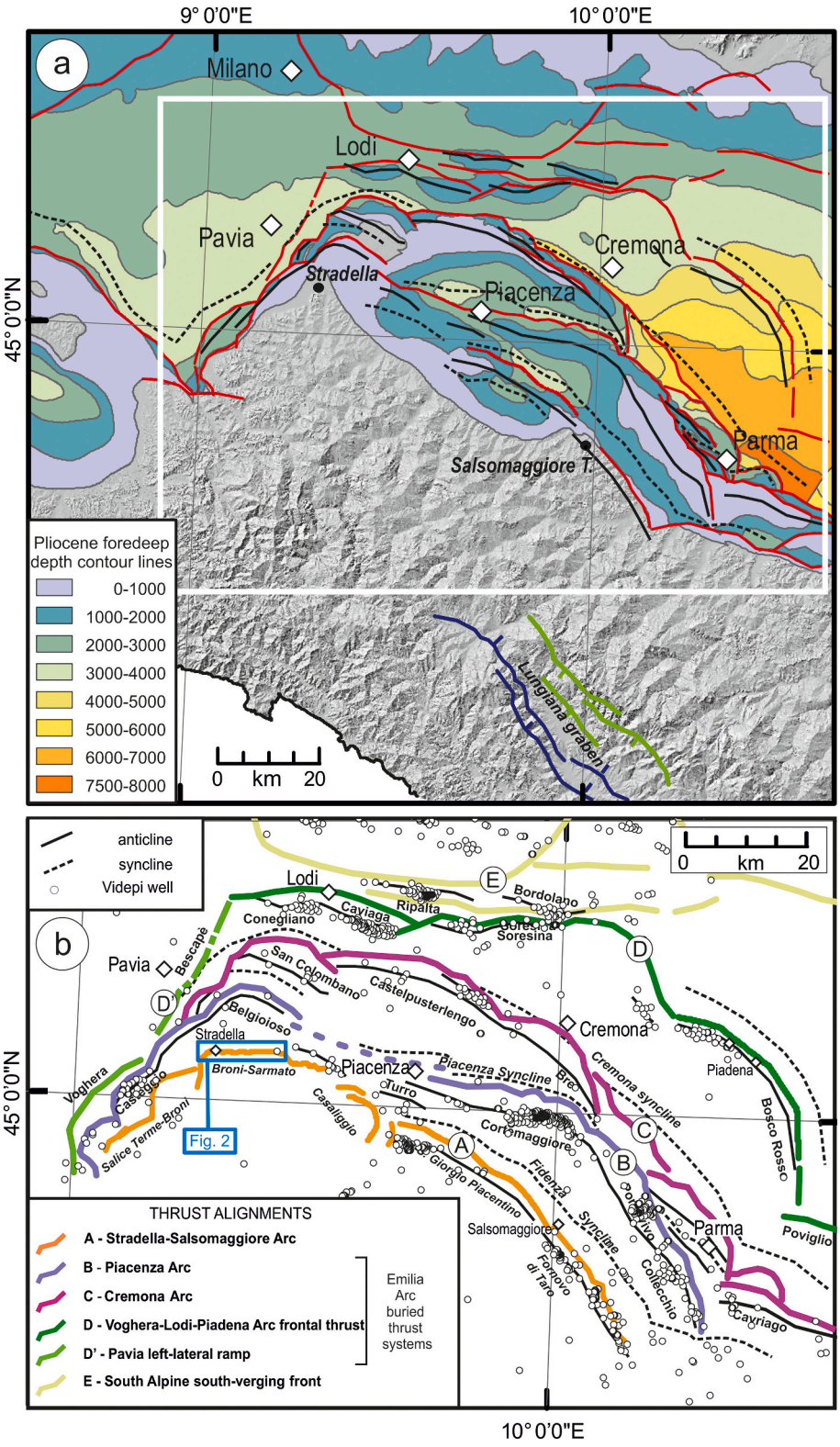

Fig. 6. GIS reconstruction of regional thrust alignments in the Emilia Arc region. a) Depth contour lines of the Pliocene Padanian foredeep deposits redrawn and georeferenced from Structural Model of Italy (scale 1:500.000) (Bigi et al., 1990); traces of associated buried thrust and fold hinges are reported. White rectangle is detailed in panel b. b) Major thrust alignments based on integrating information from the above map, Videpi well distribution, other available regional maps (Pieri and Groppi, 1981; Martelli et al., 2017), and a large number of geological cross-sections reported in Figs. S3 with references. The thrust front of the Stradella-Salsomaggiore Arc is largely outcropping; all the others are almost exclusively buried. In the blue box, the Broni-Sarmato scarp shown in Fig. 2b. (For interpretation of the references to colour in this figure legend, the reader is referred to the web version of this article.)

perfectly follow the full extent of the principal scarp, emerging only locally; in some sectors, the minor scarp coincides with boundaries of farmland, whereas in other sectors, it is in the middle of homogeneous cultivated fields (e.g., in Fig. 8d) and thus it does not coincide with farmland boundaries. A possible reason for the high discontinuity of the second scarp could be the anthropogenic activity in the area and the presence of several farmlands.

iii) To measure in detail the height of the two scarps, along the Broni-Sarmato structure we made 30 perpendicular to scarp high-precision topographic profiles (examples in Figs. 8a-c) acquired by GPS instruments. We integrated these data with 31 profiles obtained by the LiDAR images (Fig. S6). The height values of the main scarp, obtained as vertical distance of the terraces separated by the scarp, range up to 25.8 m, while those of the minor scarp range from 0.55 to 3.85 m.

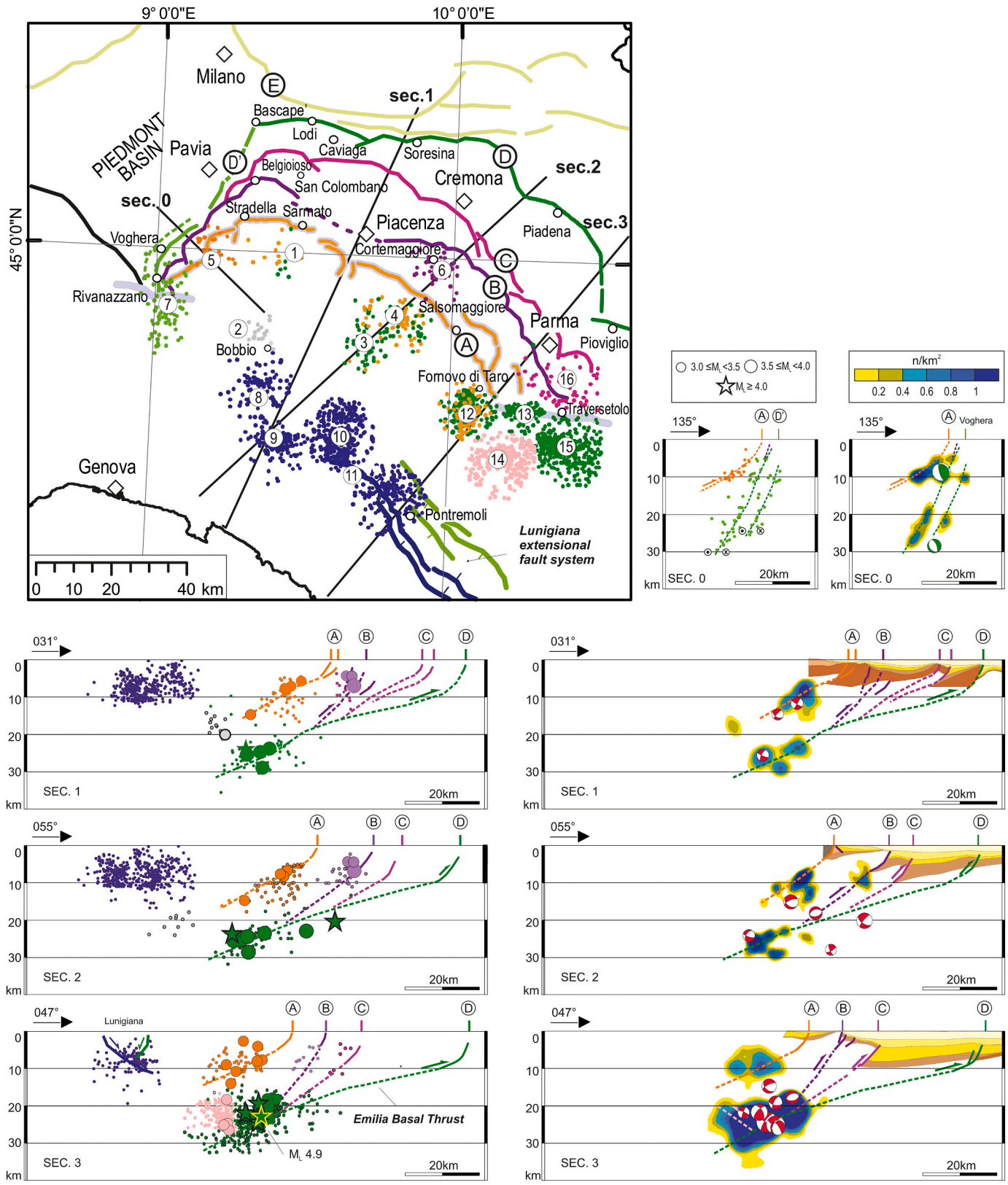

Fig. 7. Map and section-view of seismicity clusters (time period 1985–2020; 0.4 ≤ ML ≤ 4.9; depth 0–74 km) and their possible association with the Stradella-Salsomaggiore Arc and various thrusts making up the Emilia Arc. Clusters are numbered as in Fig. 4; thrust alignments are those in Fig. 6 (for further details and references, see Figs. 6, S3, and S4). In the section view, earthquakes are magnitude-scaled on the left and represented as density contours on the right; focal mechanisms are those in Fig. 5 and Table 1; the geological sections are from Pieri and Groppi (1981) (see Fig. S4 for details and key).

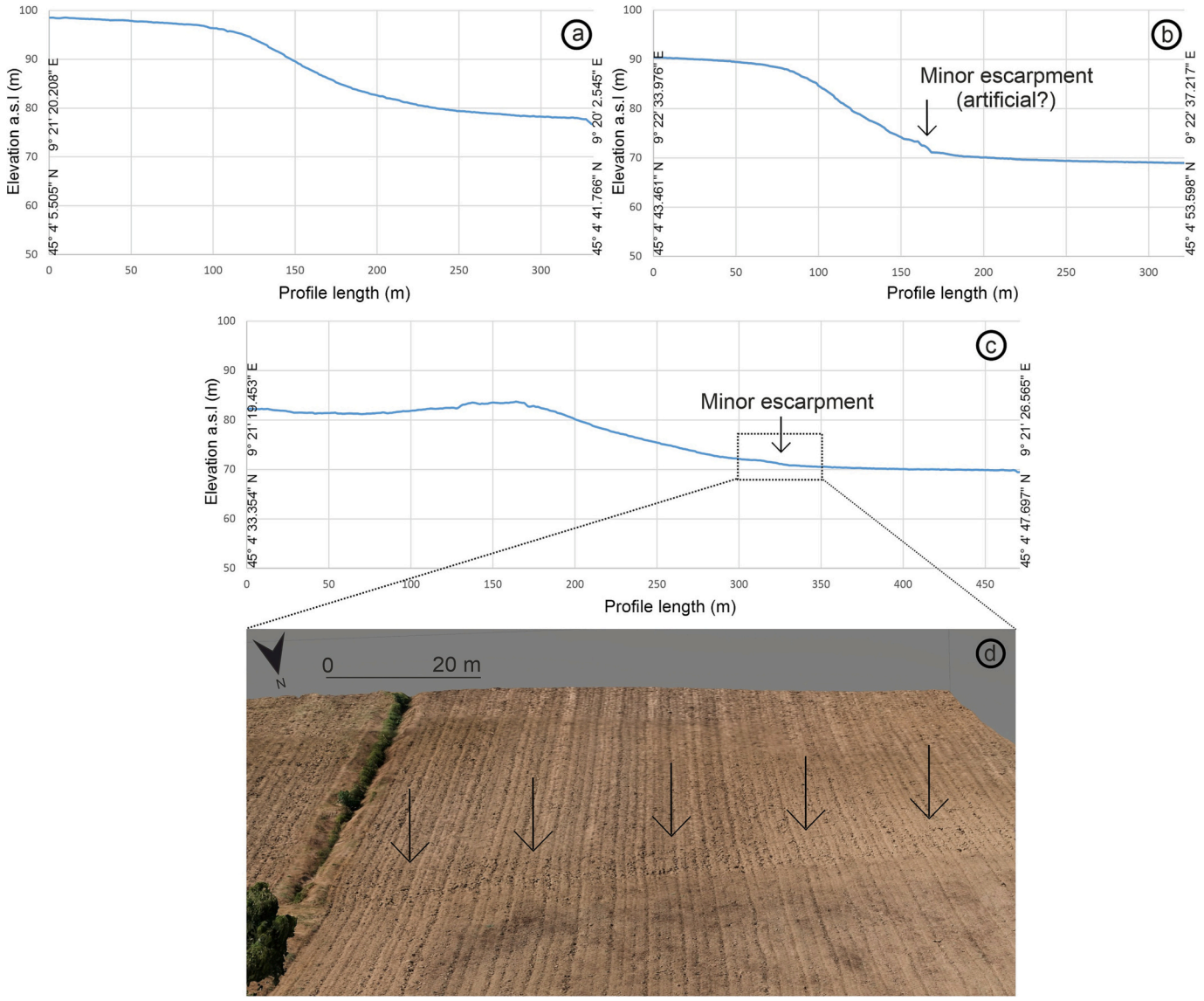

Fig. 8. Examples of high-precision GPS profiles collected along the Broni-Sarmato fault-scarp. See location in Fig. 2c. Coordinates of the tips of the profiles are shown. Arrows point to the minor scarp. d) 3D model of the secondary scarp reconstructed from drone survey. Arrows point to the 1-m-high scarp.

iv) With the DTM from LiDAR data we reconstructed the along-strike profile of the main scarp (Fig. 9b). Most of the low values measured along the profile are in zones where the original scarp has been partially eroded by river activity or correspond to right- or left-stepping zones where the scarp height was originally lower. As a whole, the values of the scarp height tend to decrease eastward, with several irregularities.

4.2. Geoelectrical surveys

Three NNE-SSW directed Electrical Resistivity Tomography (ERT) profiles were acquired across the Broni-Sarmato fault-scarp at two selected test sites, referred to as Valle Muto and Pavesa (profile traces in Fig. 2c).

In the inverse resistivity models (Fig. 10), warm colours (from green to red) are associated with freshwater-saturated clayey-to-sandy deposits, cool colours (from purple to blue) are associated with brackish water-saturated sandy deposits or freshwater-saturated clays. This is consistent with results from Torrese and Pilla (2021) who carried out a geophysical study for the delineation of aquifer geometry and the detection of saline paleo-water contaminations at a test site located about ten kilometers away from our study area. This is also consistent with results from Pilla and Torrese (2022) who carried out an integrated hydrochemical and geophysical study of the saline paleo-water uprising into the alluvial aquifer over a larger area.

The obtained geoelectrical images point out the presence of zones of the subsoil affected by brackish water contaminations (Fig. 10). The origin of these Na—Cl rich waters is connected to the brines (very high-density fluids) that are remnants of evaporated marine waters in the late Messinian (Late Miocene), trapped at the bottom of the Po Plain aquifer (Conti et al., 2000). The uprising of saline waters is facilitated by these structural discontinuities which represent preferential flow paths and facilitate the flow towards the surface and the mixing of deep saline waters with shallow fresh waters (Pilla et al., 2010; Torrese and Pilla, 2021; Pilla and Torrese, 2022). This is evident from the low resistivity values (purple colour) that are found along the discontinuities A, D, E in Fig. 10, and that extend towards the surface, on profiles ERT1 and ERT2 and even on the more detailed profile ERT3.

Horizontal interruption and vertical dislocation of a shallow, high resistivity layer (dislocated into Z and Y, X and W bodies in Fig. 10) allowed the recognition of structural discontinuities B, C and F in Fig. 10. These discontinuities appear to be associated with the uprising of brackish water to a lesser extent than the other discontinuities, as

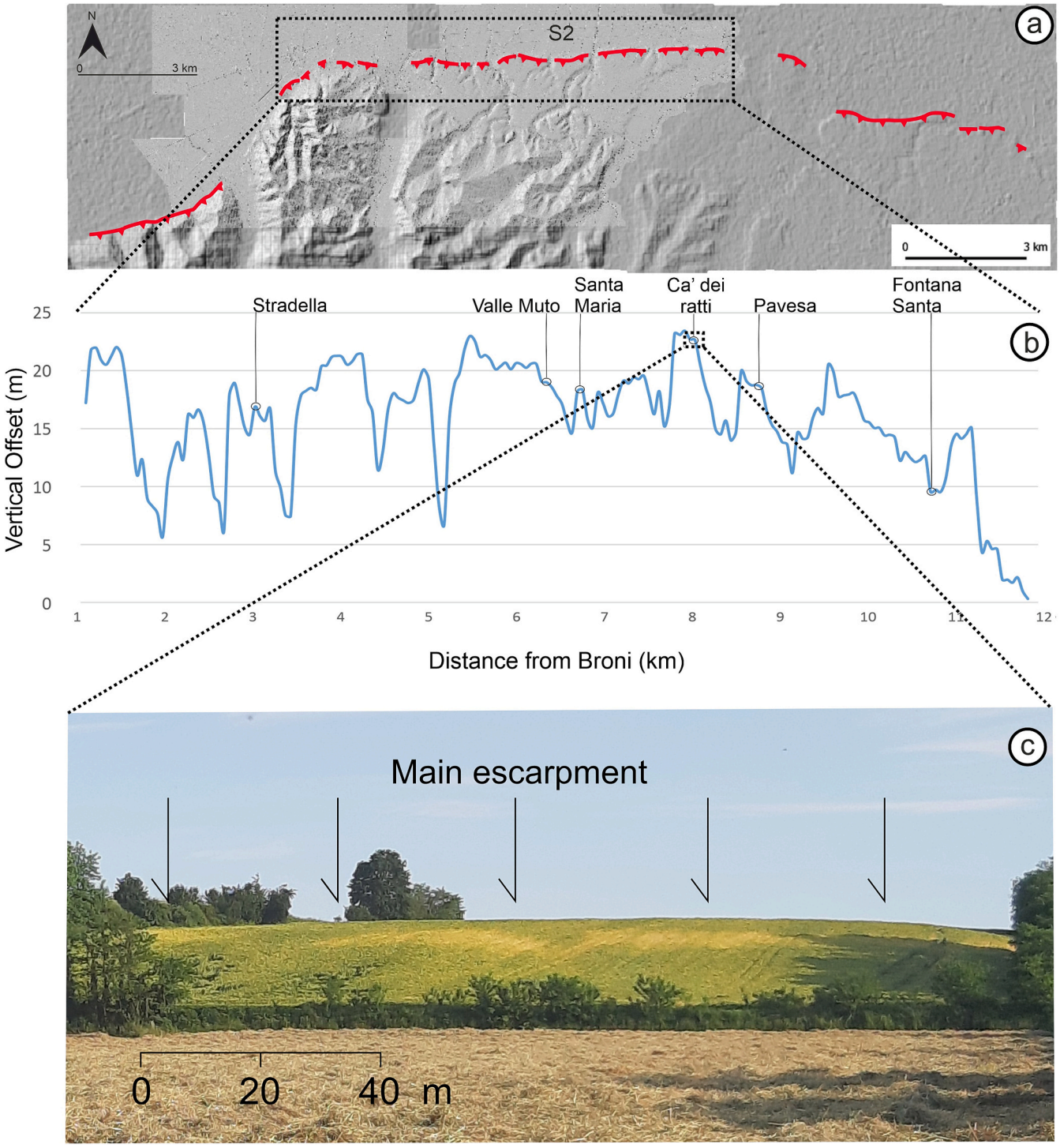

Fig. 9. a) DSM of the study area. b) Long topographic profile near parallel to the Broni-Sarmato fault-scarp, projected on E-W direction. Vertical exaggeration is 133×. The profile shows the asymmetrical variation in height of the main scarp and its along-strike segmentation. c) particular of the main scarp viewed from the north.

revealed by the detailed profile ERT3.

Among the discontinuities revealed by the inverse resistivity models we identified the main discontinuity (A) which is clearly recognizable on all profiles. Discontinuity A is associated with minor structures B and C which are found on all the profiles; other two small, shallow structures (Fig. 10) are revealed by ERT3 alone. Integrating the topographic analysis and the geoelectrical profiles, we identify the Broni-Sarmato segment as a wide zone of deformation at the shallowest level extending from point B to point D in Profile ERT1 of Fig. 10. The depth of investigation of the profiles is not enough to understand if and how these structures possibly merge at deeper level.

4.3. Earthquake distribution and kinematics

The analyzed instrumental seismicity (Figs. 3–5), occurring in the 1985–2020 time interval, is characterized by small-to-moderate-sized earthquakes with magnitude $0.1 \leq M_L \leq 4.9$ and a low seismicity rate. In instrumental time, unlike the Ferrara Arc, which experienced the

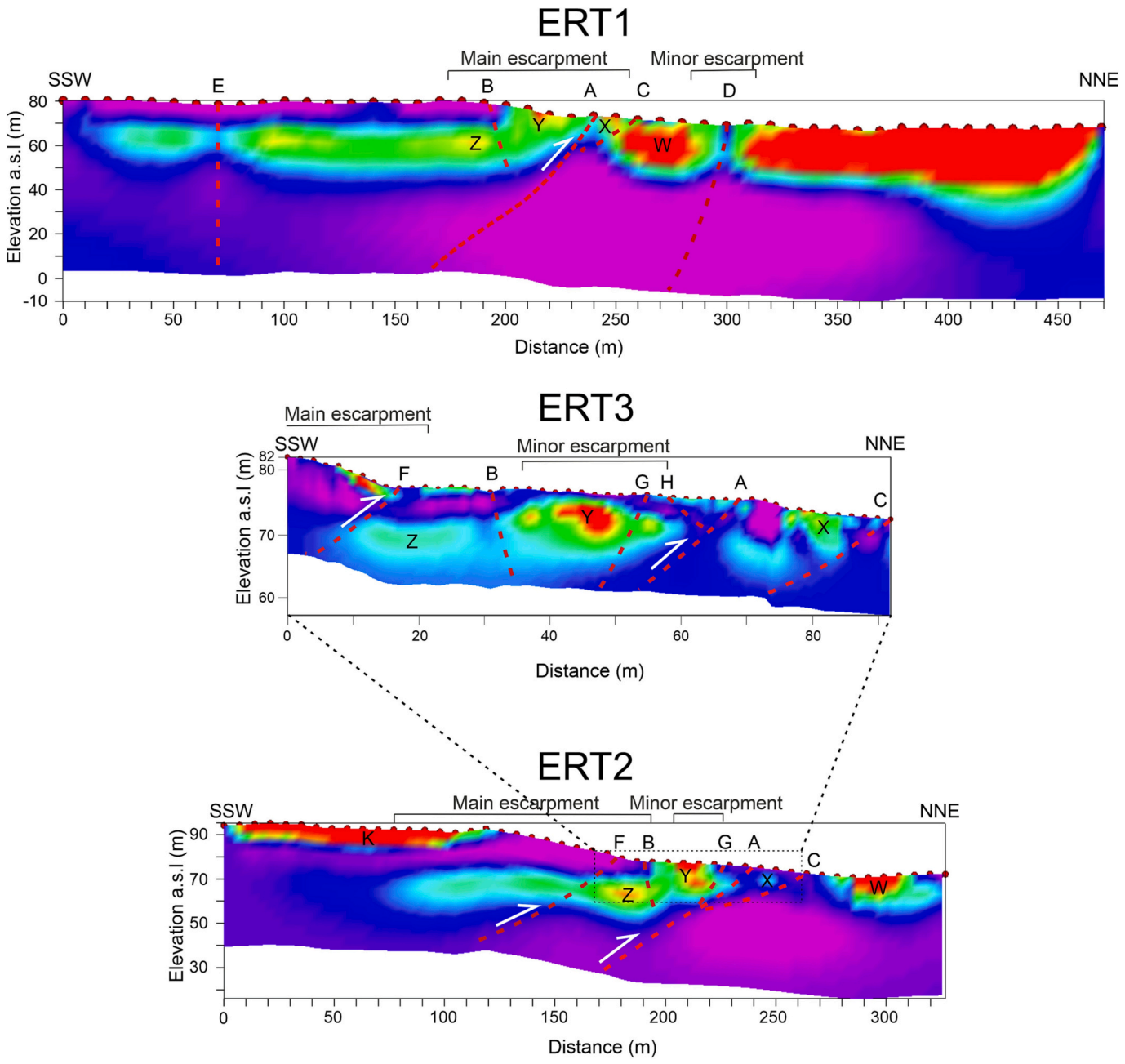

Fig. 10. Electrical Resistivity Tomography (ERT) profiles with different length, depth of investigation and resolution, acquired across the studied Broni-Sarmato deformation zone in NNE-SSW orientation. For location see Fig. 2c. The profiles are roughly orthogonal to the fault-scarps. Profile ERT1 is the longest (length 470 m), Profile ERT2 is shorter (329 m), providing great depth of investigation down to about 70 m and 50 m, respectively. Profile ERT3 is the shortest (94 m), providing high accuracy at shallow depths of about 15 m. Vertical to horizontal scale exaggeration for the profile ERT3 is 3×.

2012 Emilia seismic sequence (Mw 6.1), the study area was not affected by significant seismic activity but only by minor events that never exceeded magnitude M_L 4.9 (Fig. 3a). The major seismic sequence occurred in December 2008 at lower crustal depths (~20 km, M_L 4.9). The other event of M_L 4.9 that affected the area occurred in 2012 at a sub-crustal depth (60 km).

The completeness magnitude of the Italian Seismic Bulletin (1985–2020) is about M_L 2.4 (Fig. 3e), and although the National Seismic Network (RSN) improved significantly after 2005 and 2009 (Amato and Mele, 2008; Schorlemmer et al., 2010), better-quality earthquake detection capabilities and the lowering of the earthquake catalog completeness threshold, was observed only after 2015 (from ~ M_L 2.5 – to - ~ M_L 1.8). The parameters of the Gutenberg–Richter relationship (GR), are estimated from the available data, i.e., the annual a value (4.35) and b value (1.17).

The frequency–depth histogram of Fig. 3b, computed considering the seismicity over the completeness magnitude, depicts a bimodal pattern with maxima centered around 8 km and 26 km. About 70% of the events occur within the upper crust at depths less than ~12 km. About 30% occur within the lower crust, at depths between 12 and 30 km, and the remaining 2% occur at subcrustal depths. From an energy release point of view, we can observe that also the deepest events, albeit in much smaller numbers, in the analyzed time window, have magnitude comparable to the shallower ones (Fig. 3b).

Due to the seismic network configuration, the shallow seismicity (<10–12 km) along the Emilia Arc is not well constrained, while the deeper earthquakes, prevailingly occurring at lower crustal depths (20–30 km), as well as the events occurring in the southern part of the study area are better located (Fig. S1).

The seismicity is not uniformly distributed but instead clustered in specific zones, mainly close to known active faults (Fig. 4a). Moreover, it is much less frequent in the western part of the study area with respect to the eastern part. The cluster analysis (Fig. 4a and b) highlights 16 groups characterized by different energy release (ER) and mainly located in the study area's south-eastern portion (Fig. 4c).

The compilation of 34 FMs from the literature and 7 from this study (Tables 1 and S1; FMs with yellow border in Figs. 5 and S2) highlights three distinct kinematic domains. The seismic events with reverse solutions are predominant in the central-eastern sector of the study area at the lower crust and subcrustal depths (see red-bordered group of FMs in Fig. 5). The southern-western events present a normal kinematics compatible with the northward prosecution of Lunigiana extensional fault systems (Fig. 5a); the strike-slip solutions characterize the western flank of the outer buried front of the Emilia Arc. The P and T average kinematics axes show a sub-horizontal SSW–NNE and SW-NE- trend, respectively (Fig. 5a and b).

The average focal mechanisms for each cluster or set of clusters, computed with the Bingham statistics (Allmendinger et al., 2012), are detailed in Fig. 4b. Taking into account the epicentral distribution and prevailing depth range and kinematics, it is possible gathering the clusters into the following groups:

1- shallow tensional clusters (8, 9, 10, 11), along with the termination and northward prosecution of the Lunigiana extensional fault system (Figs. 4a, 5a);

2- shallow compressional clusters (1, 4, 12), on the hanging-wall side of the Stradella-Salsomaggiore Arc;

3- shallow compressional clusters (6, 16), on the footwall side of the Stradella-Salsomaggiore Arc;

4- lower crust compressional clusters with almost pure dip-slip kinematics and an average NE-SW P-axis (3, 12, 13, 14, 15), localized in the footwall of the Stradella-Salsomaggiore Arc;

5- shallow to lower crust strike-slip clusters (5 and 7) in the Emilia Arc's north-western side possibly associated with the Pavia left-lateral ramp (Fig. 6), with NNE-SSW-trending P-axis.

5. Unknown attribution (Cluster 2)

Cluster 6, located between Parma and Piacenza towns, and cluster 15, with reverse kinematics, are the most significant clusters in energy released among shallow and deeper earthquakes, respectively M_L max 4.0, 1991 and M_L max 4.9, 2008 in Fig. 3a.

The western extensional shallow clusters (8, 10, 11) are characterized mainly by swarms of tens of days of durations and energy less than the ones released in the eastern groups. For example, cluster 10 is the most significant in terms of n° earthquakes per unit area, but not of energy. The described extensional clusters show NE-SW trending T-axes.

5.1. 3D fault model

Following the conceptual procedural steps illustrated in Section 3.4, we reconstructed, in a georeferenced frame, the 2D and 3D geometry and kinematics of the largely outcropping Stradella-Salsomaggiore Arc and the buried various thrusts making up the Emilia Arc. We did not further analyze the extensional seismological data of the Lunigiana area, as they were out of our target.

5.1.1. Fault alignments and segmentation

The Stradella-Salsomaggiore Arc (SSA in Fig. 1 and A in Fig. 6b) extends for about 120 km along the strike. Following the thrust hierarchy proposed by Caputo and Tarabusi (2016), it may be defined as a second-order structure of the PTF. From west to east, it is articulated along strike in two third-order structures: Stradella Arc (S1, S2, and S3) and Salsomaggiore Arc (S4 and S5). In turn, the latter are organized in fourth-order individual thrust segments (S1 = Salice Terme-Broni, S2 = Broni-Sarmato, S3 = Casaliggio; S4 = San Giorgio Piacentino, S5 = Fornovo di Taro) (A in Fig. 6b). In this paper as in the literature (Benedetti et al., 2003; DISS Working Group, 2021), the generic term Stradella thrust includes segments S1 and S2.

The Emilia Arc is a thrust system having a more complex fault pattern and consisting of three well-distinguished arcuate thrust alignments. From south to north, we call them:

- Piacenza Arc (Rivanazzano-Belgioioso-Piacenza- Cortemaggiore-Soragna) (B in Fig. 6b),
- Cremona Arc (Sant'Angelo Lodigiano-San Colombano-Cremona-Parma) (C in Fig. 6b),
- Voghera-Lodi-Piadena Arc (Voghera-Lodi-Caviaga-Soresina-Piadena) (D-D′ in Fig. 6b).

The along-strike continuity of the thrust front of the Piacenza Arc also its central portion, although not so evident, may be inferred from the extent of the Piacenza syncline at its footwall (Fig. 6a).

The Voghera-Lodi-Piadena alignment bounds outward the Emilia Arc and consists of the lateral Pavia ramp (D′ from Voghera to Bescapè), with prevailing left-lateral kinematics, and of the Lodi to Piadena frontal thrust (D). As a matter of fact, all arcs have an asymmetric shape, with a longer NE side and a shorter NW side. This configuration is controlled by an ESE-dipping high-angle oblique-slip (left-lateral and dip-slip) shear zone bordering the west side of all arcuate alignments. Following Caputo and Tarabusi (2016) criteria, it may be classified as a second-order structure of the Adriatic-Padan arcuate belt. Along strike it is articulated in third-order structures. From west to east, we identify the Pavia lateral ramp along the Voghera-Bescapè alignment, the Cornegliano-Caviaga thrust, the Soresina Arc, and the Piadena arc, as shown in Fig. 6 and schematised in Fig. S7.

As observed in other sectors of the outer Apennine fold-and-thrust belt, the timing of the onset of the thrust alignments rejuvenates northward and outward from Late Miocene to Late Pliocene and Quaternary (Ghielmi et al., 2010; Livani et al., 2018; Amadori et al., 2019; Panara et al., 2021).

5.1.2. Depth geometry definition

The hypocentral distribution of seismic events and the focal

mechanisms allow us to identify cluster of seismicity with reverse/strike-slip kinematics mainly concentrated in the ranges 8–12 km and 20–30 km along the down-dip prosecution of the identified fault alignments as shown in Fig. 7.

The highest densities and the most energetic events, which occurred between 1985 and 2020, are mainly located within the lower crust (clusters 3, 12, 13, 14, 15, 16), except the Cortemaggiore seismic sequence (1991, $M_{W\ max}$ 4.0, cluster 6) occurred within the upper crust. The section-view depth geometry and the possible earthquake/fault association are evident in the four transects of Figs. 7 and 11 and along the eleven radial cross-sections of Fig. S5.

The westernmost transect (sec. 0) shows that at depths between 5 and 30 km, the seismicity can be correlated with high-angle strike-slip deformation along the Voghera segment of the Pavia transfer fault. At upper-crustal depths, it also correlates with the SSE-dipping Broni segment (S1 in Fig. 12) of the Stradella-Salsomaggiore Arc.

Transects 1 and 2 show that at upper crust depths (< 12–14 km), the earthquake activity is relatively well connected with both the SSW-dipping San Giorgio Piacentino segment (S4 in Fig. 12) of the Stradella-Salsomaggiore Arc and the nearly parallel SSW-dipping Piacenza Arc. In contrast, at lower crustal depth (17–18 km to 30–32 km), the seismicity can be well correlated with the lower crust segment of the outer front of the Emilia Arc along the down dip-prosecution of the Lodi-Piadena Arc (D) and, eventually, the lowermost portions of its splays (B and C) (Fig.7). Transect 3 highlights an SSW-dipping significant clustering between 20 and 30 km that can be associated with the outer front of the Emilia Arc (Figs. 11–13).

In summary, based on the seismicity clustering, the more energetic seismic events, and focal mechanisms, we highlight that at a depth between16–22 km, the basal thrusts of the three Emilia arcuate alignments (B, C and D-D′) merge on a common basal detachment from here onwards called Emilia Arc Basal Thrust (EBT). At depths from 17 to 18 km to 30–32 km, the EBT itself is seismogenic. On the contrary, the Stradella-Salsomaggiore Arc, does not converge with EBT but identify an independent low-angle thrust. In any case, the earthquake distribution highlights synchronous activity in the present times of both regional arcs.

The reconstructed 3D fault model of the Emilia Arc consists of three major near-parallel and well-distinct thrust surfaces (Piacenza Arc, Cremona Arc, Voghera -Lodi-Piadena Arc). Axial culmination and depression or sharp lateral bends characterize the along-strike extent of such arcuate structures, which thus result in being articulated in smaller individual segments. At lower crust depth, the three arcs are connected with a common basal detachment, here referred to as Emilia Arc Basal Thrust (EBT), which propagates with staircase trajectories from the Permian-Triassic basement (15–16 km depth) up to near-surface depths, with a characterizing fault-propagation fold-structural style as those of the Ferrara Arc (Astiz et al., 2014; Lavecchia et al., 2015).

The Lodi-Piadena frontal thrust of the Emilia Arc (e.g., D in Fig. 12) extends for about 130 km in the average WNW-ESE direction and propagates down-dip to depths of ~30–32 km, with an average dip-angle of 25°. The Pavia left-lateral ramp (D′ in Fig. 12) extends for about 50 km in the NNE-SSW direction with an average SE-dip of 70° down to depths of ~30–32 km. The southern portion is illuminated by a distinct earthquake volume associated with focal mechanisms with near pure left-lateral strike-slip kinematics (Fig. 7).

The frontal and lateral thrusts of the Emilia Arc cross the entire crust with a thick-skinned style, deforming from top to bottom Cenozoic terrigenous successions, Cenozoic and Mesozoic carbonate successions, Triassic evaporites, and underlying crystalline basements. Well-evident

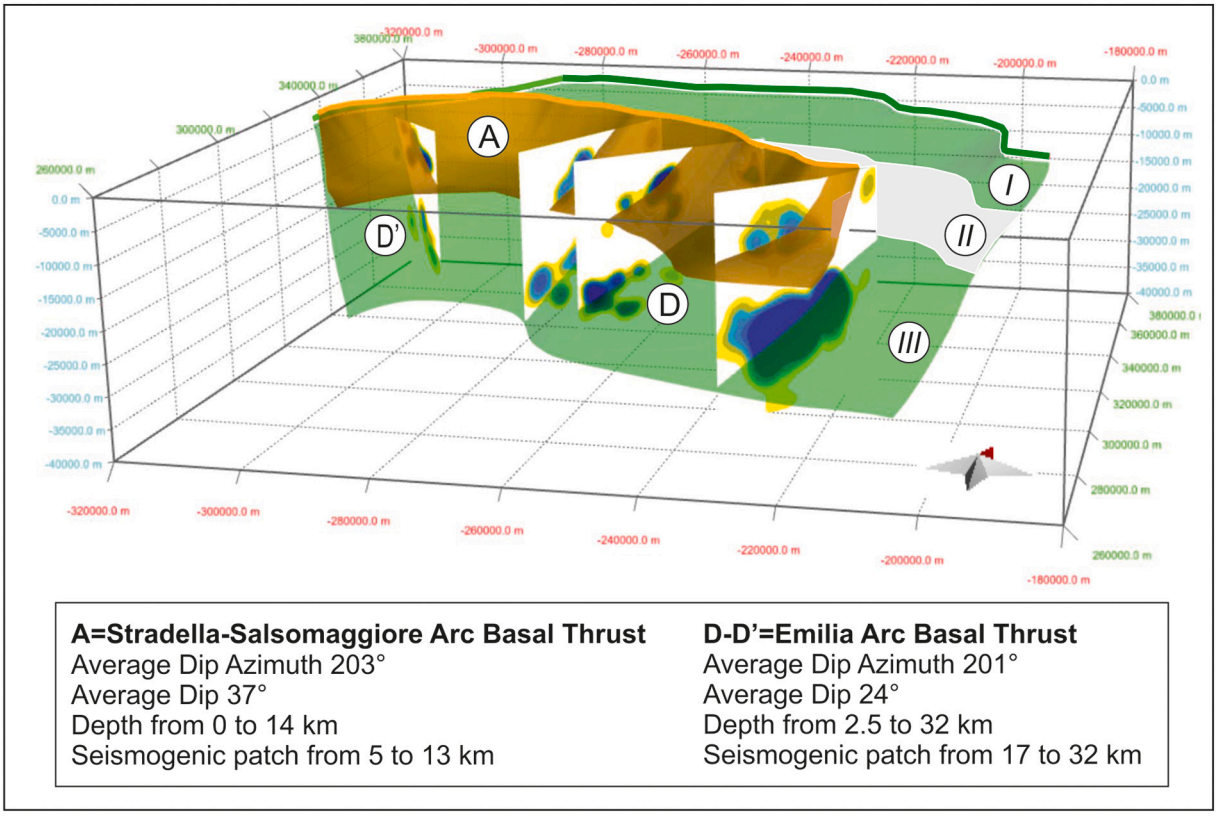

Fig. 11. 3D nonplanar fault models of the Stradella-Salsomaggiore Arc (A) and Emilia Arc Basal Thrusts (D-D′) as reconstructed in this paper integrating geological and seismological data. The two thrusts surfaces are intersected with the earthquake density contour profiles elaborated along the hypocentral sections 0, 1, 2, 3 in Fig. 10. Along dip, the outer structure of Emilia Arc consists of (I) an upper crust portion shallower than 5–6 km, that have been interpreted from geological maps and transects (Voghera-Lodi-Piadena Arc in Figs. 6b, S3 and S5); (III) a lower crust portion, between 17 and 18 and 31–32 km, built from earthquake distributions in section views (EBT in Figs. 12 and S5); (II) an intermediate portion graphically interpolated between the previous two (EBT in Fig. 12).

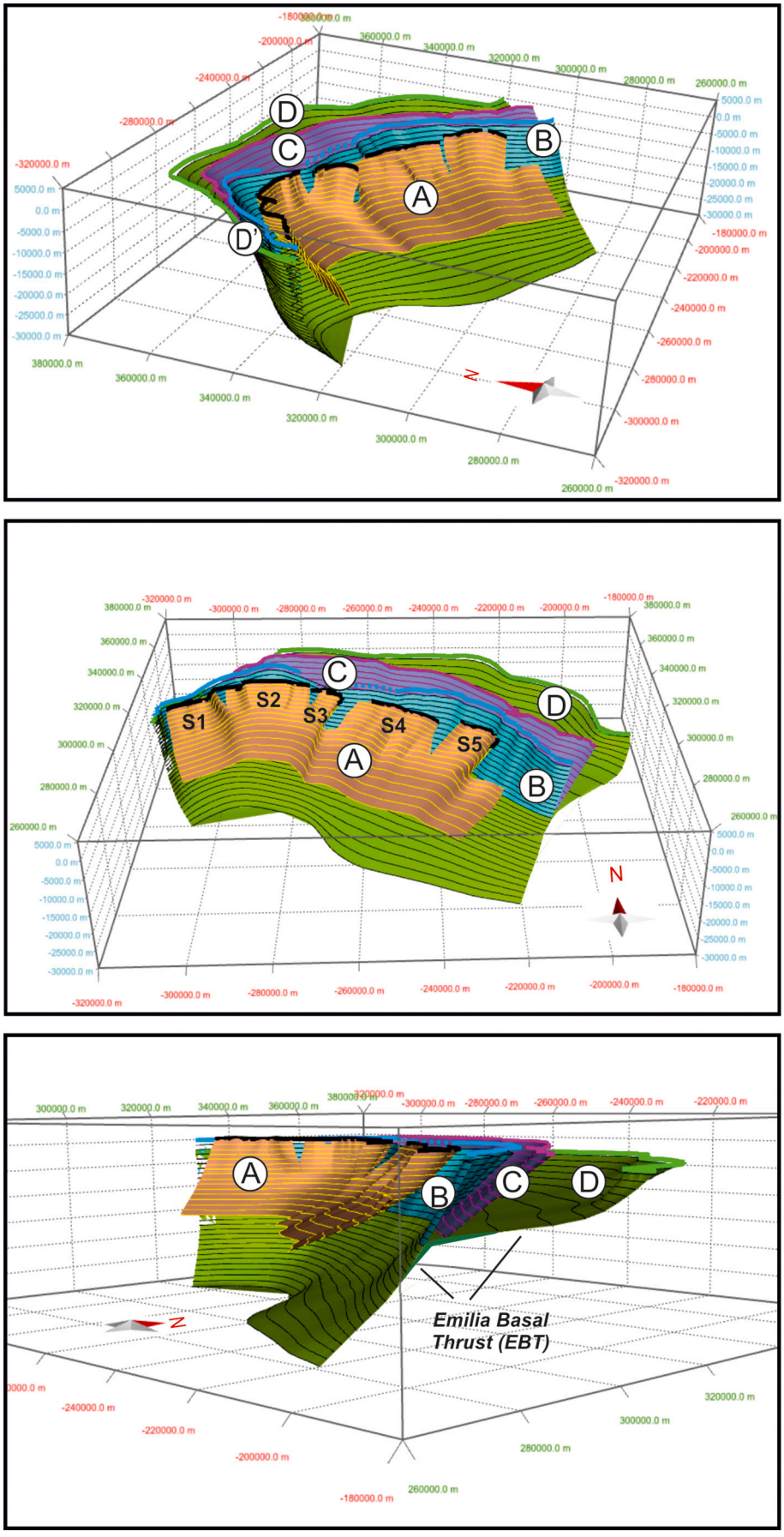

Fig. 12. Different perspective views of 3D fault models of the Stradella-Salsomaggiore Arc (A) and the Emilia Arc. The latter consists of 3 three major thrust surfaces (B=Piacenza Arc, C=Cremona Arc, D-D′ = Voghera-Lodi-Piadena Arc) splaying from the common EBT. The depth contour lines drawn on the fault surfaces are spaced 1 km and are shallower than 14 km for the Stradella-Salsomaggiore Arc and 32 km for the Emilia Arc. The segmentation of Stradella-Salsomaggiore Arc is also shown: S1 = Salice Terme-Broni, S2 = Broni-Sarmato, S3 = Casaliggio, S4 = San Giorgio Piacentino, S5 = Fornovo di Taro.4.4.3 3D fault model.

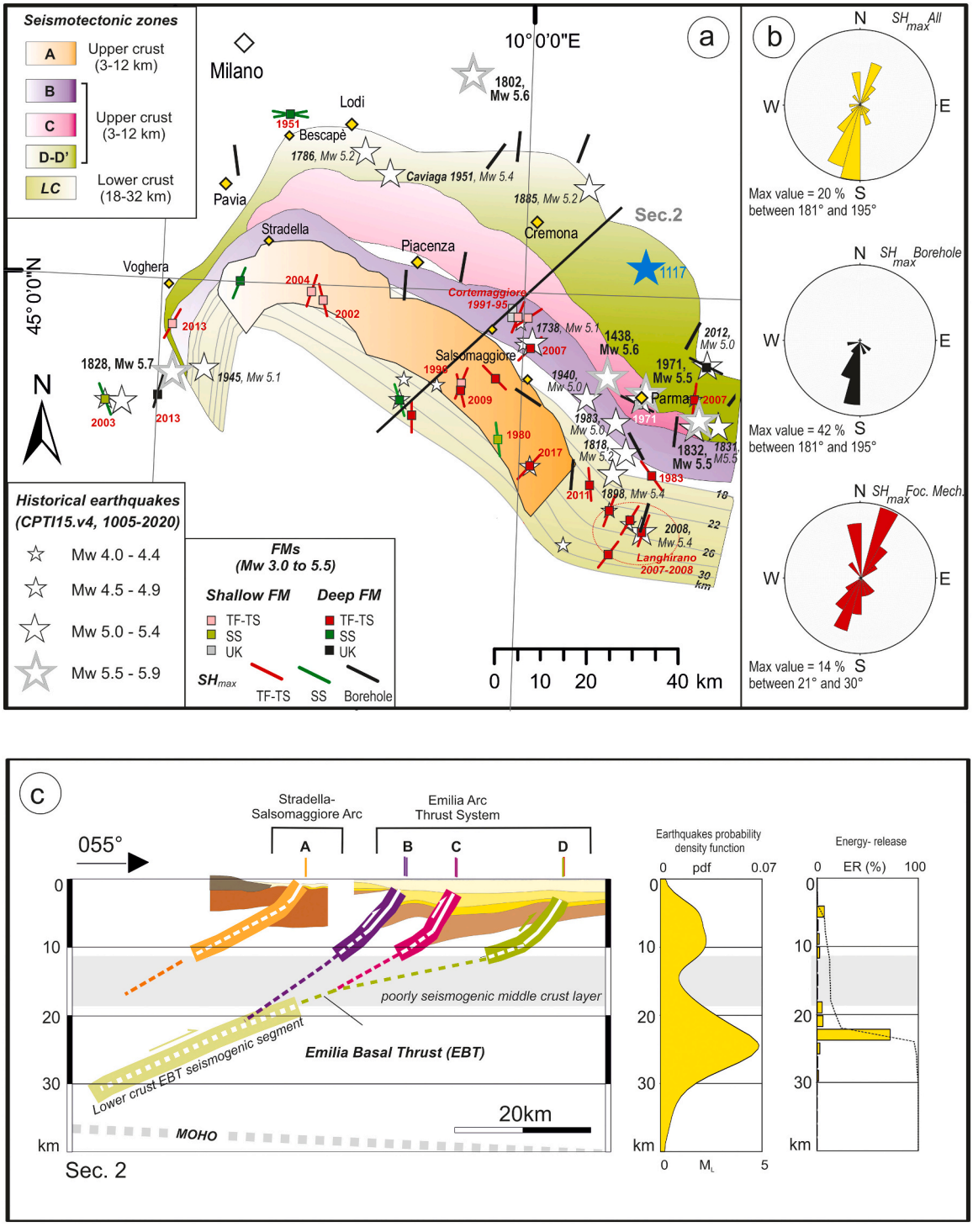

Fig. 13. Seismotectonic synoptic view of the Stradella-Salsomaggiore Arc and of the Emilia Arc. a) Seismotectonic zones corresponding to the map-view of the nonplanar fault models built in Fig. 12 and schematised in Fig. S7, with their quality ranks: A = Upper crust Stradella-Salsomaggiore Arc; B = Upper crust Piacenza Arc, C = Upper crust Cremona Arc, D-D′ = upper crust Voghera-Lodi-Piadena Arc, LC = lower crust portion of the Emilia Arc Basal Thrust (EBT). The white stars represent the historical seismicity from Rovida et al. (2022); the blue one is the Cremonese event inferred by Galli (2005). Events with Mw ≥ 4.0 are shown only for earthquakes after 1985. Data on focal mechanisms (FMs) are derived from the compilation and kinematic classification performed in this paper (Table 1), and the FMs are furtherly subdivided into two groups: shallow = upper crust (<12–14 km) and deep = lower crust (15 to 35 km). They are represented in terms of location and Maximum Horizontal Stress direction (σ_{Hmax} - colored bar); black bars are σ_{Hmax} from Borehole Breakouts (Mariucci and Montone, 2020). b) Rose-diagram representation of maximum horizontal stress as derived from the focal mechanisms (red), borehole breakouts (black), and merged dataset (yellow). c) Section-view of the 3D fault surfaces of Fig. 12 along the trace of Section 2, with some shallow geological detail and with schematic mechanical layering: the upper crust geologic limits are redrawn from Pieri and Groppi (1981) and correspond to section number 7 in Fig. S5; the Moho depth boundary is derived from Di Stefano et al. (2009). The two diagrams on the right represent the depth distribution of the instrumental seismicity and the energy released by the events lying within the boundaries of the seismotectonic zones given on the map. (For interpretation of the references to colour in this figure legend, the reader is referred to the web version of this article.)

compressional seismogenic patch characterizes the central and eastern areas of the frontal thrust at depths between ~18 and 32 km (Fig. 11; Fig. S7).

The Stradella-Salsomaggiore Arc extends along strike for about 110 km and propagates along dip to depths of about 14 km, with an average dip-angle of 25° (Figs. 7 and 11).

5.1.3. Fault model building validation

Following the criteria specified in section 3.4 (Step 5), we assigned to different depth intervals of each surface of the 3D Fault model (Fig. 12), a quality ranking based on the availability and quality of geological and seismological input and on the coherence between them (Fig. S7 and Tables S2). As a result, the surfaces at the upper crust (0–12 km) and the lower crust (18–32 km) were classified as Constrained (C), Poor Constrained (PC) and Inferred (I). Generally, no information was available at mid-crust depths, and the corresponding fault surfaces were inferred by interpolating the upper crust and lower crust geometries. Fig. S7 gives a map-view representation of the available constraints on the fault model's geometry based on evaluated seismological constraints derived from background seismicity and clusters.

6. Discussion

6.1. The Stradella thrust

About 20 years ago, Benedetti et al. (2003) highlighted the possible recent activity of the Stradella thrust at the northwestern termination of the Pede-Apennine thrust front (PTF). The tectonic origin of the Stradella scarp versus natural (gravitational) or anthropogenic processes is still questioned (DISS Working Group, 2021).

Based on the seismic interpretation by Pieri and Groppi (1981), Benedetti et al. (2003) associate the investigated fault scarp with a south-dipping high-angle thrust active since the late Messinian that branches from the Emilia Arc Basal Thrust at a depth of about 10 km. Toscani et al. (2006) interpreted the Stradella structure as a fault-related anticline developed in Messinian times at the hanging wall of the Pede-Apennines frontal thrust, and displaced in Late Pliocene-Pleistocene by two north-dipping back-thrusts detaching from the south-dipping Emilia Arc Basal Thrust.

The link at depth of the Stradella thrust and, in general, of the PTF with the Emilia Arc are controversial. Two different interpretations have been proposed: 1) the Stradella thrust and the whole PTF represent a splay structure branching at ca. 10 km-depth from a major basal detachment (Pieri and Groppi, 1981), which is common also to the outer splays/frontal ramps in the frame of a thin-skinned tectonic style. 2) The PTF, to which the Stradella thrust belongs, is associated with a thick-skinned tectonic style and intersects the active basal detachment at about 20–25 km depth (Bonini, 2013).

In this paper, we contribute to the above discussion, at the local and regional scale, on one side zooming with a morphotectonic and geoelectric approach on a particularly well-exposed segment of the Stradella thrust, i.e., the Broni-Sarmato fault-scarp, on the other side modelling the 3D geometry at depth of the Stradella thrust by integrating seismological and geological data.

6.1.1. The Broni-Sarmato fault-scarp

Recent tectonic activity along this scarp was indicated by previous authors based on geological and geomorphological surface evidence (Pellegrini and Vercesi, 1995; Benedetti et al., 2003).

Our integrated geomorphologic-geoelectric study of the Broni-Sarmato fault-scarp (Fig. 2) supports its tectonic origin and shows a sub-soil image of the fault near-surface deformation zone. Furthermore, the offset of the terraces, and the presence of hanging valleys and triangular facets along the scarp, and the diffuse presence of over-incised river valleys in the block south of the scarp, are all morphostructures classically ascribed to recent tectonic fault scarps (McCalpin, 2009; Tibaldi et al., 2017; Tibaldi and Ferrari, 1992).

We add that the scarp is linear in map view, with a number of small left- and right-stepping geometries, and one large right-stepping. These steps are characterized by gradually decreasing scarp height at the tips of the onlapping segments, a geometry incompatible with the Broni-Sarmato scarp's river origin.

We also recognize a minor scarp, with a length of 13.5 km located at the footwall of the main one. Most segments of this minor scarp are located at the boundaries of farmlands. Although we recognize the presence of deformation in the sub-soil image in the geoelectric profiles, we are more inclined to consider that the minor scarp might be instead of anthropogenic origin.

The main scarp zone corresponds to a strip of near-surface deformation, where shallow fault splays may be present, as found elsewhere (e.g., Ghisetti et al., 2007). In the Broni-Sarmato case, this geometry is consistent with the presence of several electrical discontinuities in the same zone as highlighted by the geophysical surveys (Fig. 5). The extent of brackish water contamination at depth revealed by the long geoelectrical survey (profile ERT1 in Fig. 5) suggests the presence of a wide zone of deformation that represents a preferential flow path for deep saline waters and facilitates the flow towards the surface. The extent of brackish water contamination is comparable to that reported by Torrese and Pilla (2021) and Pilla and Torrese (2022) and related to another important tectonic discontinuity located 5–10 km NNW of Stradella, in the Oltrepò Pavese plain sector (Po Valley, Northern Italy) (Fig. 1 in Torrese and Pilla, 2021). Even this tectonic discontinuity, buried below alluvial deposits, is responsible for the uprising of deep, saline paleowaters. Although the brackish water contamination does not provide any direct evidence of the recent Broni-Sarmato segment activity, we stress that there are other more direct clues coming from the geoelectrical surveys, which are the horizontal interruptions and vertical dislocations of a shallow, high resistivity layer (Fig. 10). These features are present along the geoelectrical surveys at sites located in correspondence of the major scarp, indicating possible deformation along SSW-dipping high-angle discontinuities.

Taking into account that the deformed deposits belong to unit T0, and that the uplifted units T1-T3 have a Middle-latest Pleistocene age (Benedetti et al., 2003), our geoelectrical surveys are consistent with the conclusions of these authors that along the Broni-Sarmato scarp there is the presence of shallow deformation of tectonic origin that lasted until the latest Pleistocene and, probably, the Holocene.

6.1.2. The Stradella-Salsomaggiore Arc

The Broni-Sarmato scarp represents the central E-W segment of the Stradella Arc (Figs. 2a and 6) as reconstructed in this paper integrating the available geologic and seismologic information (Figs. 2, 6b). The Stradella Arc continues towards SE with the Salsomaggiore Arc (Figs. 6 and 12). According to our reconstruction, the overall Stradella-Salsomaggiore Arc consists of five along-strike well-distinguished fault segments, possibly laterally interconnected at a depth of about 5 km (Fig. 12) and belonging to the PTF. All five segments show an evident westward-dipping low-angle seismogenic volume at a depth between a few kilometers and 12–14 km, along with the down-dip prosecution of their surface trace (Figs. 7 and S5). The Salice Terme-Broni and San Giorgio Piacentino segments (S1 and S4) show the most relevant association with instrumental seismicity (Fig. S5). Information on the earthquake kinematics is limited to a few compressive focal solutions with an average NNE-striking P-axis associated with the Salice Terme-Broni (S1), Broni-Sarmato (S2), San Giorgio Piacentino (S4) and Fornovo di Taro segments (S5) (Fig. S7, Table S2).

Although a modest seismic activity, available earthquake data are all geometrically and kinematically coherent to constrain the overall Stradella-Salsomaggore Arc as an upper crustal structure, thus excluding a direct connection with the underlying EBT.

6.2. The Emilia Arc

According to our 3D reconstruction (Figs. 11 and 12), a characterizing geometric seismotectonic feature of the Emilia Arc is a regional scale well-evident lower crust basal detachment that undergoes seismogenic compression at depths between 18 and 32 km (Figs. 7 and S5). This tectonic structure is here called the Emilia Arc Basal Thrust (EBT) (Fig.13) and may be geometrically reconnected with the outer front of the Emilia Arc (Voghera-Lodi-Piadena Arc). Some more internal upper crust segments (Cremona and Piacenza Arcs) splaying from the EBT are highlighted from geological interpretations of seismic lines (e.g., transects in Figs. 7 and S4). Overall, the Emilia Arc depicts a thick-skinned tectonic style for this sector of the Northern Apennines.

Although only a few earthquake data are attributed to the Emilia Arc within upper crustal depths, we identify at least two shallow clusters (number 6 and 16 in Fig. 7 and Table S3) that indicate shallow activity along the splay structures. Similar thick-skinned crust-scale geometries with an alternance of seismic and aseismic layers and the presence of a poorly seismogenic middle crust layer, have already been observed along the Marche-Adriatic Arc, where it is also constrained by a near vertical seismic reflection profile (Lavecchia et al., 2003, 2007; Visini et al., 2010; de Nardis et al., 2022).

Although more schematic, Turrini et al. (2015) highlighted a similar thick-skinned style, identifying sub-crustal seismicity across the Po Valley basin linked to the deep propagation of near-surface thrusts.

In contrast, Vannoli et al. (2015) points out that the Northern Apennines deep crust earthquakes are not directly related to upper crust thrust tectonics but independently occur below the basal detachment of the Northern Apennines and represent subduction-related settings. In particular, the DISS 3.3.1 database (DISS Working Group, 2021) reconstruction shows subduction-related depth contour at depths between 8 and 20 km, lying more or less beneath the PTF hanging wall area. Furthermore, the seismic dataset analyzed in this paper (Figs. 7 and S5) suggests that such depth interval corresponds to a poorly seismogenic crustal layer (Fig. 13).

A different interpretation of the Emilia and Ferrara Arcs is proposed by Livani et al. (2018) based on boreholes and seismic lines. These Authors describe the arcs as thin-skinned salient-recess configurations, consisting of an alternate of advanced and less advanced segments, controlled by the pre-existing paleogeographic configuration and progressively developed during the outward growth of the system (Ghielmi et al., 2010). Costa (2003) attributes the non-cylindrical deformation to lateral strike-slip deformation paths that control differential shortening along the frontal and lateral segments.

Different from DISS Working Group (2021), but following Martelli et al. (2017), we stress the regional seismotectonic role and relevance of the Voghera-Lodi-Piadena Arc (D-D′ in Figs. 6, 7 and 12) along its overall extent and at multi-depths. In conclusion, we confirm and detail the evidence of an earthquake stratigraphy highlighted by Turrini et al. (2015) and characterized by at least two distinct syn-kinematic seismogenic layers, one within the mainly Mesozoic sedimentary succession and the other across the upper part of the lower crust.

6.3. Inferences for a new seismotectonic zonation

The 3D fault models built for the Stradella-Salsomaggiore and the Emilia Arc (Figs. 11 and 12) represent relevant results that could contribute to revising the seismotectonic zonation for SHA analyses. For example, in Fig. 13a, the identified seismotectonic zones correspond to the map-view projection of the upper (3 to 12 km) and lower (18 to 34 km) crust portions of the nonplanar fault surfaces reconstructed in Fig. 12.

Both the Stradella-Salsomaggiore Arc and the Emilia Arc show ongoing deformation coherent with a regional NNE-oriented compression, thus implying dip-slip kinematics along the SSW-dipping structures, a minor right-lateral component on the SW-dipping segments, a prevailing left-lateral strike-slip component along the ESE-dipping Pavia transfer fault.

The historical seismicity (Mw >4, 1005–2020, Rovida et al., 2020) is projected on the map together with the focal mechanisms (Mw 3 to 5.5) analyzed in this paper (Fig. 4) and with the borehole breakouts (Mariucci and Montone, 2020), represented as maximum horizontal stress. The areal distribution of these data highlights as the historical and instrumental activity is mainly focused on the southeastern sector of the area, in association with NNE-directed compression of both the upper and lower crust of the Emilia Arc structures, and, subordinately, with the Salsomaggiore Arc.

In particular, a concentration of moderate events is observed at the hangingwall of SW-dipping segments of Piacenza and Cremona Arc between the localities of Cortemaggiore and Parma (1438, Mw 5.6; 1738, Mw 5.1; 1818, Mw 5.2; 1898, Mw 5.4; 1940, Mw 5.0; 1971, Mw 5.5; 1983, Mw 5.0; 1991–1995). Conversely, the Reggio Emilia 1831 (Mw 5.5) and 1832 (Mw 5.5) events and the 2007–2008 Langhirano deep earthquakes (Mw 5.4) are better correlated with the SSE-dipping segment of the EBT.

The moderate seismicity characterizing the Lodi-Piadena area (e.g., Pianura Lombarda 1786, Mw 5.2; Pianura Lombarda 1885, Mw 5.0), including the 3 January 1117 destructive Cremonese event (Galli, 2005), might be attributed to the shallow upper crustal segments of the outer Emilia Arc front (e.g., the Lodi Piadena Arc), as similarly observed for the Ferrara Arc (Lavecchia et al., 2015). Considering the proposed reconstruction, we wonder whether, similarly to the Oltrepò Pavese events occurred in 1828 (Mw 5.7) and 1945 (Mw 5.1), the Caviaga 1951 strike-slip earthquake (Mw 5.4, depth ~ 30–32 km, Caciagli et al., 2015; Peruzza et al., 2021), might be attributed to the activation at lower crust depth of the Pavia left-lateral ramp, rather than to the south-Alpine thrust (see Fig. S5). Alternatively, whenever it would have a shallow depth (5 km, Caloi et al., 1956), it might have been released to the Lodi-Piadena Arc.

Fig. 13 offers a view of the proposed geologic model and seismotectonic zonation, summarizing the information in the paper. The two diagrams on the right of the c panel represent the depth distribution of the instrumental seismicity and energy released by the events lying within the boundaries of the seismotectonic zones given on the map and well support the proposed seismogenic layering.

In light of the availability and quality of input data, some seismotectonic supply maps are offered in the supplementary material with a specific quality zoning and a corresponding excel data table to validate the proposed model.

7. Conclusions

The paper is an example of a multi-scale and interdisciplinary structural approach to the seismotectonics of a poorly exposed and slowly deforming region at the outer front of an orogenic belt in a highly populated and industrialized region relevant for seismic risk evaluation.

The local problem is implementing the information on the near-surface geometry, the sub-soil image, and down-dip prosecution of a debated seismogenic thrust source (Stradella thrust), whose Late Quaternary fault-scarp is exposed for a length of ~40 km not far from the metropolis of Milan (Italy), along the southern border of the populated Po Plain. The regional problem is to frame the debated Stradella thrust, which belongs to the Stradella-Salsomaggiore portion of the Late Miocene-Quaternary Pede-Apennine thrust front, in the 3D geometric, kinematic and seismotectonic context of the Late Pliocene-Quaternary Emilia Arc in the Northern Apennines.

Results and open problems are summarized in the following points:

1) Integrated morphotectonic and geoelectric analyses of the Stradella fault support the tectonic thrust-related origin of the structure and details the exposed and sub-soil geometry (Figs. 2, 8–10).

2) Hypocentral data illuminate the down-dip prosecution of the Stradella thrust to depths of 12–14 km along an SSW-dipping low-angle discontinuity (Fig.7).
3) Hypocentral data illuminate a low-angle regional structure, defined as Stradella-Salsomaggiore Arc (SSA), that includes the Stradella thrust and extends along the Pede-Apennines thrust front (PTF) for about 120 km along strike and 12–14 km along dip (Figs. 7). It has an average dip-angle of 25° and never converges at depth with the underlying Emilia Arc Basal Thrust. The SSA fault geometry is relatively homogeneously defined, but only a few compressional focal mechanisms indicate the ongoing kinematics.
4) Hypocentral data illuminate the Emilia Arc Basal Thrust (EBT) at depths between 18 and 32 km, highlighting the potentially relevant seismogenic role of both the frontal, reverse, and the lateral strike-slip, thrust segments (D and D1 in Fig. 12).
5) Geological and seismological data in a 3D framework highlight a thick-skinned style of the Quaternary and active compressional deformation for the Emilia Arc, with a basal thrust developing across the entire crust (Figs. 11 and 12).
6) The mechanical layering strongly controls the Emilia Arc seismic release, and it is mainly concentrated within the upper crust (<12 km) and the upper part of the lower crust (18–32 km).
7) Since historical times, the upper crust fault segments of the Emilia Arc appears to be silent with respect to the lower crust ones. Nevertheless, we do not forget that the neighboring Ferrara Arc was almost aseismic at upper crust depth until May 2012, when it suddenly released a destructive multi-event thrust sequence.

Finally, we wish to stress that in the case of slowly deforming and blind fault systems, a multi-scale and multi-disciplinary methodological approach is suitable to solve the seismotectonic puzzle, at least in part, and to contribute to a better knowledge of the individual structures capable of producing seismic hazards and risk in populated areas.

Credit authorship contribution statement

Dual-first authorship for Alessandro Tibaldi and Rita de Nardis: both Conceptualization, Data analysis, Writing – original draft, Review. Patrizio Torrese: collection and interpretation of geoelectrical data. Sofia Bressan: Data collection. Martina Pedicini: Data collection. Donato Talone: Data collection and 3D fault model building. Fabio L. Bonali: Data collection. Noemi Corti: Data collection. Elena Russo: Data collection. Giusy Lavecchia: Structural analysis, 3D fault model building and seismotectonic interpretation.

Declaration of Competing Interest

The authors declare that they have no known competing financial interests or personal relationships that could have appeared to influence the work reported in this paper.

Data availability

Data will be made available on request.

Acknowledgments

We acknowledge the useful suggestions of three anonymous reviewers and Riccardo Caputo on an earlier version of the manuscript. *Research activities have been carried out in the frame of the Italian PRIN Project (Research Projects of National Interest)* "Fault segmentation and seismotectonics of active thrust systems: the Northern Apennines and Southern Alps laboratories for new Seismic Hazard Assessments in northern Italy (NASA4SHA)" *(PI R. Caputo, UR Responsible A. Tibaldi),* of the CRUST - Interuniversity Center for 3D Seismotectonics with Territorial Applications, and under the aegis of the International Lithosphere Program, Task Force II. We acknowledge PetEx that provided the Move 2019.1 suite software license and we thank Daniele Spallarossa and his colleagues for providing us the waveforms of the Regional Seismic Network of Northwestern Italy RSNI.

Appendix A. Supplementary data

Supplementary data to this article can be found online at https://doi.org/10.1016/j.tecto.2023.229853.

References

Aki, K., 1965. Maximum likelihood estimate of b in the formula log N= a-bM and its confidence limits. Bull. Earthquake Res. Inst.Tokyo Univ. 43, 237–239.
Allmendinger, R.W., Cardozo, N.C., Fisher, D., 2012. Structural Geology Algorithms: Vectors and Tensors. Cambridge University Press, Cambridge, England, p. 289.
Amadori, C., Toscani, G., Di Giulio, A., Maesano, F.E., D'Ambrogi, C., Ghielmi, M., Fantoni, R., 2019. From cylindrical to non-cylindrical foreland basin: Pliocene–Pleistocene evolution of the Po Plain–Northern Adriatic basin (Italy). Basin Res. 31, 991–1015. https://doi.org/10.1111/bre.12369.
Amato, A., Mele, F.M., 2008. Performance of the INGV National Seismic Network from 1997 to 2007. Ann. Geophys. 15.
Anderson, H., Jackson, J., 1987. Active tectonics of the Adriatic Region. Geophys. J. Int. 91, 937–983. https://doi.org/10.1111/j.1365-246X.1987.tb01675.x.
Astiz, L., Dieterich, J.H., Frohlich, C., Hager, B.H., Juanes, R., Shaw, J.H., 2014. On the potential for induced seismicity at the Cavone oilfield: analysis of geological and geophysical data, and geomechanical modeling. Report for the Laboratorio di Monitoraggio Cavone (139 pp).
Baddeley, A., Rubak, E., Turner, R., 2015. Spatial Point Patterns: Methodology and Applications with R. CRC Press, Boca Raton, FL, USA (ISBN 1482210215).
Bally, A.W., Burbi, L., Cooper, C., Ghelardoni, R., 1986. Balanced sections and seismic reflection profiles across the Central Apennines. Mem. Soc. Geol. It. 35, 257–310.
Barchi, M.R., Beltrando, M., 2010. The Neogene-Quaternary evolution of the Northern Apennines: crustal structure, style of deformation and seismicity. J. Virtual Explor. 36 (10).
Basili, R., Barba, S., 2007. Migration and shortening rates in the northern Apennines, Italy: implications for seismic hazard. Terra Nova 19, 462–468. https://doi.org/10.1111/j.1365-3121.2007.00772.x.
Bello, S., de Nardis, R., Scarpa, R., Brozzetti, F., Cirillo, D., Ferrarini, F., di Lieto, B., Arrowsmith, R.J., Lavecchia, G., 2021. Fault Pattern and Seismotectonic Style of the Campania – Lucania 1980 Earthquake (Mw 6.9, Southern Italy): New Multidisciplinary Constraints. Front. Earth Sci. 8, 608063 https://doi.org/10.3389/feart.2020.608063.
Benedetti, L., Tapponnier, P., King, G.C.P., Meyer, B., Manighetti, I., 2000. Growth folding and active thrusting in the Montello region, Veneto, northern Italy. J. Geophys. Res. 105, 739–766. https://doi.org/10.1029/1999JB900222.
Benedetti, L.C., Tapponnier, P., Gaudemer, Y., Manighetti, I., Van der Woerd, J., 2003. Geomorphic evidence for an emergent active thrust along the edge of the Po Plain: the Broni-Stradella fault: EVIDENCE FOR AN EMERGENT THRUST ALONG THE PO PLAIN. J. Geophys. Res. 108 https://doi.org/10.1029/2001JB001546.
Bennett, R.A., Serpelloni, E., Hreinsdóttir, S., Brandon, M.T., Buble, G., Basic, T., Casale, G., Cavaliere, A., Anzidei, M., Marjonovic, M., Minelli, G., Molli, G., Montanari, A., 2012. Syn-convergent extension observed using the RETREAT GPS network, northern Apennines, Italy: NORTHERN APENNINES DEFORMATION. J. Geophys. Res. 117 https://doi.org/10.1029/2011JB008744 n/a-n/a.
Bigi, G., Cosentino, D., Parotto, M., Sartori, R., Scandone, P. (Eds.), 1990. Structural Model of Italy (1:500.000), CNR-Progetto finalizzato geodinamica, Sheets 1 e 2. SELCA, Firenze.
Boccaletti, M., Coli, M., Eva, C., Ferrari, G., Giglia, G., Lazzarotto, A., Merlanti, F., Nicolich, R., Papani, G., Postpischl, D., 1985. Considerations on the seismotectonics of the Northern Apennines. Tectonophysics 7–38.
Boccaletti, M., Corti, G., Martelli, L., 2011. Recent and active tectonics of the external zone of the Northern Apennines (Italy). Int J Earth Sci (Geol Rundsch) 100, 1331–1348. https://doi.org/10.1007/s00531-010-0545-y.
Bonali, F.L., Tibaldi, A., Marchese, F., Fallati, L., Russo, E., Corselli, C., Savini, A., 2019. UAV-based surveying in volcano-tectonics: an example from the Iceland rift. J. Struct. Geol. 121, 46–64.
Boncio, P., Bracone, V., 2009. Active stress from earthquake focal mechanisms along the Padan–Adriatic side of the Northern Apennines (Italy), with considerations on stress magnitudes and pore-fluid pressures. Tectonophysics 476, 180–194. https://doi.org/10.1016/j.tecto.2008.09.018.
Bonini, M., 2013. Fluid seepage variability across the external Northern Apennines (Italy): Structuralcontrols with seismotectonic and geodynamic implications. Tectonophysics 590, 151–174.
Brunsdon, C., 1995. Estimating probability surfaces for geographical point data: an adaptive kernel algorithm. Comput. Geosci. 21, 877–894.
Burrato, P., Ciuffi, F., Valensise, G., 2003. An inventory of river anomalies in the Po Plain, Northern Italy: evidence for active blind thrust faulting. Ann. Geophys. 46 https://doi.org/10.4401/ag-3459.
Caciagli, M., Camassi, R., Danesi, S., Pondrelli, S., Salimbeni, S., 2015. Can we consider the 1951 Caviaga (Northern Italy) Earthquakes as Noninduced events? Seismol. Res. Lett. 86, 1335–1344. https://doi.org/10.1785/0220150001.

Caloi, P., Panfilis, M., Filippo, D., Marcelli, L., Spadea, M.C., 1956. Terremoti della Val Padana del 15-16 maggio 1951. Ann. Geofis. 9, 63–105. https://doi.org/10.4401/ag-5594.
Caputo, R., Tarabusi, G., 2016. Il complesso sistema di sorgenti sismogeniche nell'area ferrarese ei loro effetti nella storia. In: ATTI DELL'ACCADEMIA DELLE SCIENZE DI FERRARA, vol. 93. ACCADEMIA DELLE SCIENZE DI FERRARA.
Carafa, M.M.C., Barba, S., 2013. The stress field in Europe: optimal orientations with confidence limits. Geophys. J. Int. 193, 531–548. https://doi.org/10.1093/gji/ggt024.
CARG, 2016. Carta geologica d'Italia, scale 1:50,000, Voghera sheet n.178.
Carminati, E., Doglioni, C., 2012. Alps vs. Apennines: the paradigm of a tectonically asymmetric Earth. Earth Sci. Rev. 112, 67–96. https://doi.org/10.1016/j.earscirev.2012.02.004.
Cassano, E., Fichera, R., Arisi Rota, F., 1986. Rilievo aeromagnetico d'Italia: alcuni risultati interpretativi. Atti del 5° Convegno Annuale del Gruppo Nazionale di Geofisica della Terra Solida II, 939–962.
Castaldo, R., de Nardis, R., DeNovellis, V., Ferrarini, F., Lanari, R., Lavecchia, G., Pepe, S., Solaro, G., Tizzani, P., 2018. Coseismic Stress and Strain Field Changes Investigation Through 3-D Finite Element Modeling of DInSAR and GPS Measurements and Geological/Seismological Data: The L'Aquila (Italy) 2009 Earthquake Case Study. J. Geophys. Res. Solid Earth 123, 4193–4222. https://doi.org/10.1002/2017JB014453.
Castellarin, A., Vai, G.B., 1986. South alpine versus Po plain apenninic arcs. In: Wezel, F. C. (Ed.), The Origin of Arcs. Elsevier Sci, New York, pp. 253–280.
Cazzini, F., Zotto, O.D., Fantoni, R., Ghielmi, M., Ronchi, P., Scotti, P., 2015. Oil and gas in the adriatic foreland, Italy. J. Pet. Geol. 38, 255–279. https://doi.org/10.1111/jpg.12610.
Cenni, N., Baldi, P., Mantovani, E., Ferrini, M., D'Intinosante, V., Barbucci, D., Albarello, D., 2008. Short term (geodetic) and long term (geological) velocity fields in the Northern Apennines. Bollettino della Società geologica italiana 127 (1), 93–104.
Chiarabba, C., Jovane, L., DiStefano, R., 2005. A new view of Italian seismicity using 20 years of instrumental recordings. Tectonophysics 395, 251–268. https://doi.org/10.1016/j.tecto.2004.09.013.
Ciaccio, M.G., Di Stefano, R., Improta, L., Mariucci, M.T., BSI Working Group, 2021. First-Motion Focal Mechanism Solutions for 2015–2019 M $\geq$ 4.0 Italian Earthquakes. Front. Earth Sci. 9, 630116 https://doi.org/10.3389/feart.2021.630116.
Cibin, U., Di Giulio, A., Martelli, L., 2003. Oligocene-early Miocene tectonic evolution of the northern Apennines (northwestern Italy) traced through provenance of piggy-back basin fill successions. Geol. Soc. Lond., Spec. Publ. 208, 269–287. https://doi.org/10.1144/GSL.SP.2003.208.01.13.
Cirillo, D., Totaro, C., Lavecchia, G., Orecchio, B., de Nardis, R., Presti, D., Ferrarini, F., Bello, S., Brozzetti, F., 2021. Structural complexities and tectonic barriers controlling recent seismic activity of the Pollino area (Calabria-Lucania, Southern Italy) – constraints from stress inversion and 3D fault model building (preprint). Tectonic plate interactions, magma genesis, and lithosphere deformation at all scales/Structural geology and tectonics, rock physics, experimental deformation/Tectonics. https://doi.org/10.5194/se-2021-76.
Conti, A., Sacchi, E., Chiarle, M., Martinelli, G., Zuppi, G.M., 2000. Geochemistry of the formation waters in the Po plain (Northern Italy): an overview. Appl. Geochem. 15, 51–65. https://doi.org/10.1016/S0883-2927(99)00016-5.
Costa, M., 2003. The buried, Apenninic arcs of the Po Plain and northern Adriatic Sea (Italy): a new model. Boll. Soc. Geol. Ital. 122, 3–23.
D'Anastasio, E., De Martini, P.M., Selvaggi, G., Pantosti, D., Marchioni, A., Maseroli, R., 2006. Short-term vertical velocity field in the Apennines (Italy) revealed by geodetic levelling data. Tectonophysics 418, 219–234. https://doi.org/10.1016/j.tecto.2006.02.008.
de Nardis, R., Filippi, L., Costa, G., Suhadolc, P., Nicoletti, M., Lavecchia, G., 2014. Strong motion recorded during the Emilia 2012 thrust earthquakes (Northern Italy): a comprehensive analysis. Bull. Earthq. Eng. 12, 2117–2145.
de Nardis, R., Pandolfi, C., Cattaneo, M., Monachesi, G., Cirillo, D., Ferrarini, F., Bello, S., Brozzetti, F., Lavecchia, G., 2022. Lithospheric double shear zone unveiled by microseismicity in a region of slow deformation. Sci. Rep. 12, 21066.
Delaunay, B., 1934. Sur la sphere vide. Izv. Akad. Nauk SSSR. Otdelenie Matematicheskii i Estestvennyka Nauk 7 (793–800), 1–2.
DelaVega, M., Osella, A., Lascano, E., 2003. Joint inversion of Wenner and dipole–dipole data to study a gasoline-contaminated soil. J. Appl. Geophys. 54, 97–109. https://doi.org/10.1016/j.jappgeo.2003.08.020.
DeMets, C., Gordon, R.G., Argus, D.F., Stein, S., 1990. Current plate motions. Geophys. J. Int. 101, 425–478. https://doi.org/10.1111/j.1365-246X.1990.tb06579.x.
DeMets, C., Gordon, R.G., Argus, D.F., Stein, S., 1994. Effect of recent revisions to the geomagnetic reversal time scale on estimates of current plate motions. Geophys. Res. Lett. 21, 2191–2194. https://doi.org/10.1029/94GL02118.
Devoti, R., Esposito, A., Pietrantonio, G., Pisani, A.R., Riguzzi, F., 2011. Evidence of large scale deformation patterns from GPS data in the Italian subduction boundary. Earth Planet. Sci. Lett. 311, 230–241. https://doi.org/10.1016/j.epsl.2011.09.034.
Di Stefano, R., Kissling, E., Chiarabba, C., Amato, A., Giardini, D., 2009. Shallow subduction beneath Italy: Three-dimensional images of the Adriatic-European-Tyrrhenian lithosphere system based on high-quality P wave arrival times. J. Geophys. Res. 114, B05305. https://doi.org/10.1029/2008JB005641.
DISS Working Group, 2021. Database of Individual Seismogenic Sources (DISS), Version 3.3.0: A compilation of potential sources for earthquakes larger than M 5.5 in Italy and surrounding areas. Istituto Nazionale di Geofisica e Vulcanologia (INGV). https://doi.org/10.13127/diss3.3.0.
Eva, E., Solarino, S., Boncio, P., 2014. HypoDD Relocated Seismicity in Northern Apennines (Italy) Preceding the 2013 Seismic Unrest: seismotectonic implications for the Lunigiana-Garfagnana area. B. Geofis. Teor. Appl. 55, 739–754. https://doi.org/10.4430/bgta0131.
Fantoni, R., Franciosi, R., 2010. Tectono-sedimentary setting of the Po Plain and Adriatic foreland. Rend. Fis. Acc. Lincei 21, 197–209. https://doi.org/10.1007/s12210-010-0102-4.
Ferrarini, F., Arrowsmith, J.R., Brozzetti, F., de Nardis, R., Cirillo, D., Whipple, K.X., Lavecchia, G., 2021. Late Quaternary Tectonics along the Peri-Adriatic Sector of the Apenninic Chain (Central-Southern Italy): Inspecting active Shortening through Topographic Relief and Fluvial Network analyses. Lithosphere 1–28.
Frepoli, A., Amato, A., 1997. Contemporaneous extension and compression in the Northern Apennines from earthquake fault-plane solutions. Geophys. J. Int. 129, 368–388. https://doi.org/10.1111/j.1365-246X.1997.tb01589.x.
Galli, P., 2005. I terremoti del gennaio 1117. Ipotesi di un epicentro nel cremonese. Il Quaternario 87–100.
Gasparini, C., Iannaccone, G., Scarpa, R., 1985. Fault-plane solutions and seismicity of the Italian peninsula. Tectonophysics 117, 59–78. https://doi.org/10.1016/0040-1951(85)90236-7.
Ghielmi, M., Minervini, M., Nini, C., Rogledi, S., Rossi, M., Vignolo, A., 2010. Sedimentary and tectonic evolution in the eastern Po-Plain and northern Adriatic Sea area from Messinian to Middle Pleistocene (Italy). Rend. Fis. Acc. Lincei 21, 131–166. https://doi.org/10.1007/s12210-010-0101-5.
Ghielmi, M., Minervini, M., Nini, C., Rogledi, S., Rossi, M., 2013. Late Miocene–Middle Pleistocene sequences in the Po Plain – Northern Adriatic Sea (Italy): The stratigraphic record of modification phases affecting a complex foreland basin. Mar. Pet. Geol. 42, 50–81. https://doi.org/10.1016/j.marpetgeo.2012.11.007.
Ghisetti, F.C., Gorman, A.R., Sibson, R.H., 2007. Surface breakthrough of a basement fault by repeated seismic slip episodes: the Ostler Fault, south Island. New Zealand. Tectonics 26 (6).
Gobetti, A., Perotti, C.R., 1990. Genesi e caratteristiche dell'arco strutturale di Pavia. Atti Ticinesi Scienze Terra 33, 143–156.
Govoni, A., Marchetti, A., De Gor, I.P., Di Bona, M., Lucente, F.P., Improta, L., Chiarabba, C., Nardi, A., Margheriti, L., Agostinetti, N.P., Di Giovambattista, R., Latorre, D., Anselmi, M., Ciaccio, M.G., Moretti, M., Castellano, C., Piccinini, D., 2014. The 2012 Emilia seismic sequence (northern Italy): imaging the thrust fault system by accurate aftershocks location. Tectonophysics. 622, 44–55.
Gutenberg, B., Richter, C.F., 1956. Earthquake magnitude, intensity, energy, and acceleration (second paper). Bull. Seismol. Soc. Am. 46, 138–154.
ISIDe Working Group, 2007. Italian Seismological Instrumental and Parametric Database (ISIDe). Istituto Nazionale di Geofisica e Vulcanologia (INGV). 2022 https://doi.org/10.13127/ISIDE (accessed 13 March.
Ito, K., 1999. Seismogenic layer, reflective lower crust, surface heat flow and large inland earthquakes. Tectonophysics 306 (3–4), 423–433.
LaBrecque, D.J., Miletto, M., Daily, W., Ramirez, A., Owen, E., 1996. The effects of noise on Occam's inversion of resistivity tomography data. GEOPHYSICS 61, 538–548. https://doi.org/10.1190/1.1443980.
Lavecchia, G., Boncio, P., Creati, N., 2003. A lithospheric-scale seismogenic thrust in Central Italy. Journ. Geodynamics 36, 79–94.
Lavecchia, G., De Nardis, R., Visini, F., FerrariniI, F., Barbano, M.S., 2007. Seismogenic evidence of ongoing compression in eastern-Central Italy and mainland Sicily: a comparison. Boll. Soc. Geol.It. 126, 209–222.
Lavecchia, G., De Nardis, R., Costa, G., Tiberi, L., Ferrarini, F., Cirillo, D., Brozzetti, F., Suhadolc, P., 2015. Was the Mirandola thrust really involved in the Emilia 2012 seismic sequence (northern Italy)? Implications on the likelihood of triggered seismicity effects. Boll. Geofis. Teor. Appl. 56, 461–488.
Lavecchia, G., Adinolfi, G.M., de Nardis, R., Ferrarini, F., Cirillo, D., Brozzetti, F., De Matteis, R., Festa, G., Zollo, A., 2017. Multidisciplinary inferences on a newly recognized active east-dipping extensional system in Central Italy. Terra Nova 29, 77–89. https://doi.org/10.1111/ter.12251.
Lavecchia, G., Nardis, R.D., Ferrarini, F., Cirillo, D., Bello, S., Brozzetti, F., 2021. Regional seismotectonic zonation of hydrocarbon fields in active thrust belts: A case study from Italy. In: Building Knowledge for Geohazard Assessment and Management in the Caucasus and Other Orogenic Regions. Springer, Dordrecht, pp. 89–128.
Livani, M., Scrocca, D., Arecco, P., Doglioni, C., 2018. Structural and Stratigraphic Control on Salient and recess Development along a Thrust Belt Front: the Northern Apennines (Po Plain, Italy). J. Geophys. Res. Solid Earth 123, 4360–4387. https://doi.org/10.1002/2017JB015235.
Maesano, F.E., D'Ambrogi, C., Burrato, P., Toscani, G., 2015. Slip-rates of blind thrusts in slow deforming areas: examples from the Po Plain (Italy). Tectonophysics 643, 8–25. https://doi.org/10.1016/j.tecto.2014.12.007.
Mariucci, M.T., Montone, P., 2020. Database of Italian present-day stress indicators, IPSI 1.4. Scientific data 7 (1), 298.
Martelli, L., Santulin, M., Sani, F., Tamaro, A., Bonini, M., Rebez, A., Corti, G., Slejko, D., 2017. Seismic hazard of the Northern Apennines based on 3D seismic sources. J. Seismol. 21, 1251–1275. https://doi.org/10.1007/s10950-017-9665-1.
Mazzoli, S., Helman, M., 1994. Neogene patterns of relative plate motion for Africa-Europe: Some implications for recent Central Mediterranean tectonics. In: Active Continental Margins—Present and Past. Springer, Berlin, Heidelberg, pp. 464–468.
Mazzoli, S., Santini, S., Macchiavelli, C., Ascione, A., 2015. Active tectonics of the outer northern Apennines: Adriatic vs. Po Plain seismicity and stress fields. J. Geodyn. 84, 62–76. https://doi.org/10.1016/j.jog.2014.10.002.
McCalpin, J., 2009. Paleoseismology, 2nd ed. International geophysics series. Academic Press, Burlington, MA. (629 pages).
Michetti, A.M., Giardina, F., Livio, F., Mueller, K., Serva, L., Sileo, G., Vittori, E., Devoti, R., Riguzzi, F., Carcano, C., Rogledi, S., Bonadeo, L., Brunamonte, F., Fioraso, G., 2012. Active compressional tectonics, Quaternary capable faults, and the

seismic landscape of the Po Plain (northern Italy). Ann. Geophys. 5 https://doi.org/10.4401/ag-5462.
Montone, P., Mariucci, M.T., 1999. Active stress along the external margin of the Apennines: the Ferrara arc, northern Italy. J. Geodyn. 28, 251–265. https://doi.org/10.1016/S0264-3707(98)00041-6.
Montone, P., Mariucci, M.T., 2016. The new release of the Italian contemporary stress map. Geophys. J. Int. 205, 1525–1531. https://doi.org/10.1093/gji/ggw100.
Montone, P., Mariucci, M.T., Pierdominici, S., 2012. The Italian present-day stress map. Geophys. J. Int. 189, 705–716. https://doi.org/10.1111/j.1365-246X.2012.05391.x.
Morelli, G., LaBrecque, D.J., 1996. Advances in ERT inverse model. European Journal of Environmental and Engeneering Geophysics 171–186.
Nicholson, C., Plesch, A., Sorlien, C.C., Shaw, J.H., Hauksson, E., 2014. The SCEC 3D community fault model (CFM-v5): An updated and expanded fault set of oblique crustal deformation and complex fault interaction for southern California. In: AGU Fall Meeting Abstracts (Vol. 2014, pp. T31B-4584).
Okabe, A., Boots, B., Sugihara, K., 1992. Spatial Tessellation Concept and Applications of Voronoi Diagrams. John Wiley & Sons, New York, p. 532.
Okal, E.A., 2019. Energy and Magnitude: a Historical Perspective. Pure Appl. Geophys. 176, 3815–3849.
Panara, Y., Maesano, F.E., Amadori, C., Fedorik, J., Toscani, G., Basili, R., 2021. Probabilistic Assessment of Slip rates and their Variability over Time of Offshore buried Thrusts: a Case Study in the Northern Adriatic Sea. Front. Earth Sci. 9, 664288 https://doi.org/10.3389/feart.2021.664288.
Pellegrini, G.B., Vercesi, P.L., 1995. Considerazioni morfoneotettoniche sullazona a sud del Po tra Voghera (PV) e Sarmato (PC). Atti Tic. Sci. Terra 38, 95–118.
Perotti, C., Vercesi, P.L., 1992. Assetto tettonico ed evoluzione strutturale recente della porzione nord-occidentale dell'Appennino emiliano. Mem. Descr.Carta Geol. D'It. 46, 313–326.
Peruzza, L., Schibuola, A., Romano, M.A., Garbin, M., Guidarelli, M., Sandron, D., Priolo, E., 2021. A revised image of the instrumental seismicity in the Lodi area (Po Plain, Italy). Solid Earth 12, 2021–2039. https://doi.org/10.5194/se-12-2021-2021.
Picotti, V., Pazzaglia, F.J., 2008. A new active tectonic model for the construction of the Northern Apennines mountain front near Bologna (Italy): active construction Apennines front. J. Geophys. Res. 113 https://doi.org/10.1029/2007JB005307.
Pieri, M., Groppi, G., 1981. Subsurface geological structure of the Po plain, Italy, Pubbl. In: 414, Cons. Agip, Rome, Naz. Delle Ric.
Pilla, G., Torrese, P., 2022. Hydrochemical-geophysical study of saline paleo-water contamination in alluvial aquifers. Hydrogeol. J. https://doi.org/10.1007/s10040-021-02446-5.
Pilla, G., Torrese, P., Bersan, M., 2010. Application of hydrochemical and preliminary geophysical surveys within the study of the saltwater uprising occurring in the Oltrepò Pavese plain aquifer. Boll. Geofis. Teor. Appl. 51 (4).
Plesch, A., Shaw, J.H., Benson, C., Bryant, W.A., Carena, S., Cooke, M., Yeats, R., 2007. Community fault model (CFM) for southern California. Bull. Seismol. Soc. Am. 97 (6), 1793–1802.
Pondrelli, S., Salimbeni, S., Ekström, G., Morelli, A., Gasperini, P., Vannucci, G., 2006. The Italian CMT dataset from 1977 to the present. Phys. Earth Planet. Inter. 159, 286–303. https://doi.org/10.1016/j.pepi.2006.07.008.
Pondrelli, S., Salimbeni, S., Morelli, A., Ekström, G., Postpischl, L., Vannucci, G., Boschi, E., 2011. European–Mediterranean regional centroid moment tensor catalog: solutions for 2005–2008. Phys. Earth and Planet. Inter. 185 (3–4), 74–81.
Pondrelli, S., Visini, F., Rovida, A., D'Amico, V., Pace, B., Meletti, C., 2020. Style of faulting of expected earthquakes in Italy as an input for seismic hazard modeling. Nat. Hazards Earth Syst. Sci. 20, 3577–3592. https://doi.org/10.5194/nhess-20-3577-2020.
Reasenberg, P., Oppenheimer, D., 1985. FPFIT. In: Geol, U.S. (Ed.), FPPLOT and FPPAGE: FORTRAN Computer Programs for Calculating and Displaying Earthquake Fault-Plane Solution. Surv, Open-File, Rep, pp. 85–739.
Richter, C.F., 1958. Elementary Seismology. W.H, Freeman and Company, San Francisco, CA.
Rovida, A., Locati, M., Camassi, R., Lolli, B., Gasperini, P., 2020. The Italian earthquake catalogue CPTI15. Bull. Earthq. Eng. 18, 2953–2984. https://doi.org/10.1007/s10518-020-00818-y.
Rovida, A., Locati, M., Camassi, R., Lolli, B., Gasperini, P., Antonucci, A., 2022. Italian Parametric Earthquake Catalogue (CPTI15), version 4.0. Istituto Nazionale di Geofisica e Vulcanologia (INGV). https://doi.org/10.13127/cpti/cpti15.4.
Schorlemmer, D., Mele, F., Marzocchi, W., 2010. A completeness analysis of the National Seismic Network of Italy. J. Geophys. Res. 115, B04308. https://doi.org/10.1029/2008JB006097.
Scognamiglio, L., Tinti, E., Quintiliani, M., 2006. Time Domain Moment Tensor [Data Set]. Istituto Nazionale di Geofisica e Vulcanologia (INGV). https://doi.org/10.13127/TDMTsdata.2018.49.
Serpelloni, E., Anzidei, M., Baldi, P., Casula, G., Galvani, A., 2005. Crustal velocity and strain-rate fields in Italy and surrounding regions: new results from the analysis of permanent and non-permanent GPS networks. Geophys. J. Int. 161, 861–880. https://doi.org/10.1111/j.1365-246X.2005.02618.x.
Serpelloni, E., Vannucci, G., Pondrelli, S., Argnani, A., Casula, G., Anzidei, M., Baldi, P., Gasperini, P., 2007. Kinematics of the Western Africa-Eurasia plate boundary from focal mechanisms and GPS data. Geophys. J. Int. 169, 1180–1200. https://doi.org/10.1111/j.1365-246X.2007.03367.x.
Silverman, B.W., 1986. Density estimation for statistical data analysis. Chapman & Hall, London. https://doi.org/10.1007/978-1-4899-3324-9.
Szalai, S., Novák, A., Szarka, L., 2009. Depth of Investigation and Vertical Resolution of Surface Geoelectric Arrays. JEEG 14, 15–23. https://doi.org/10.2113/JEEG14.1.15.
Takasu, T., Yasuda, A., 2009. Development of the low-cost RTK-GPS receiver with an open source program package RTKLIB. In: International Symposium on GPS/GNSS 1. International Convention Center Jeju Korea.
Tellini, C., Pellegrini, L., Castiglioni, G.B., Elmi, C., Pellegrini, G.B., 2001. Forme di origine tettonica—Tectonic landforms. Geogr. Fis. Din. Quat. 4, 55–68.
Tibaldi, A., Alania, V., Bonali, F.L., Enukidze, O., Tsereteli, N., Kvavadze, N., Varazanashvili, O., 2017. Active inversion tectonics, simple shear folding and back-thrusting at Rioni Basin, Georgia. J. Struct. Geol. 96, 35–53.
Tibaldi, A., Ferrari, L., 1992. Latest Pleistocene-Holocene tectonics of the Ecuadorian Andes. Tectonophysics 205 (1–3), 109–125.
Torrese, P., 2020. Investigating karst aquifers: using pseudo 3-D electrical resistivity tomography to identify major karst features. J. Hydrol. 580, 124257 https://doi.org/10.1016/j.jhydrol.2019.124257.
Torrese, P., Pilla, G., 2021. 1D-4D electrical and electromagnetic methods revealing fault-controlled aquifer geometry and saline water uprising. J. Hydrol. 600, 126568 https://doi.org/10.1016/j.jhydrol.2021.126568.
Toscani, G., Bonini, L., Ahmad, M.I., Di Bucci, D., Di Giulio, A., Seno, S., Galuppo, C., 2014. Opposite verging chains sharing the same foreland: Kinematics and interactions through analogue models (Central Po Plain, Italy). Tectonophysics 633, 268–282.
Toscani, G., Seno, S., Fantoni, R., Rogledi, S., 2006. Geometry and timing of deformation inside a structural arc: the case of the western Emilian folds (Northern Apennine front, Italy). Boll. Soc. Geol. It. 125, 59–65.
Tsereteli, N., Tibaldi, A., Alania, V., Gventsadse, A., Enukidze, O., Varazanashvili, O., Müller, B.I.R., 2016. Active tectonics of Central-Western Caucasus, Georgia. Tectonophysics 691, 328–344.
Turrini, C., Angeloni, P., Lacombe, O., Ponton, M., Roure, F., 2015. Three-dimensional seismo-tectonics in the Po Valley basin, Northern Italy. Tectonophysics 661, 156–179. https://doi.org/10.1016/j.tecto.2015.08.033.
Utsu, T., 1965. A method for determining the value of b in a formula log n = a – bM showing the magnitude frequency for earthquakes. Geophys. Bull. Hokkaido Univ. 13, 99–103.
Vannoli, P., Burrato, P., Valensise, G., 2015. The Seismotectonics of the Po Plain (Northern Italy): Tectonic Diversity in a Blind Faulting Domain. Pure Appl. Geophys. 172, 1105–1142. https://doi.org/10.1007/s00024-014-0873-0.
Vercesi, P. L., Falletti, P., Pasquini, C., Papani, L., Perotti, C., Tucci, G., 2015. Carta Geologica d'Italia alla scala 1:50.000. Foglio 178 'Voghera'. ISPRA, Istituto Superiore per la Protezione e la Ricerca Ambientale, 1 sheet at 1:50,000 scale and illustrative notes.
Visini, F., de Nardis, R., Lavecchia, G., 2010. Rates of active compressional deformation in Central Italy and Sicily: Evaluation of the seismic budget. Int. J. Earth Sci. 99 (Suppl. 1), 243–264.
Watts, A.B., Burov, E.B., 2003. Lithospheric strength and its relationship to the elastic and seismogenic layer thickness. Earth Planet. Sci. Lett. 213 (1–2), 113–131.
Wiemer, S., 2001. A Software Package to Analyze Seismicity: ZMAP. Seismol. Res. Lett. 72, 373–382. https://doi.org/10.1785/gssrl.72.3.373.
Wiemer, S., Wyss, M., 2000. Minimum magnitude of completeness in earthquake catalogs: examples from Alaska, the western United States, and Japan. Bull. Seismol. Soc. Am. 90 (4), 859–869.
Wilson, L.F., Pazzaglia, F.J., Anastasio, D.J., 2009. A fluvial record of active fault-propagation folding, Salsomaggiore anticline, northern Apennines. Italy. J. Geophys. Res. 114, B08403. https://doi.org/10.1029/2008JB005984.
Woessner, J., Wiemer, S., 2005. Assessing the quality of earthquake catalogues: estimating the magnitude of completeness and its uncertainty. Bull. Seismol. Soc. Am. 95 https://doi.org/10.1785/012040007.
Zhang, G., 2022. Detecting and Visualizing Observation Hot-spots in massive Volunteer-Contributed Geographic Data across Spatial Scales using GPU-Accelerated Kernel Density Estimation. ISPRS Int. J. Geo-Inf. 11, 55. https://doi.org/10.3390/ijgi11010055.
Zoback, M.L., 1992. First- and second-order patterns of stress in the lithosphere: the World stress Map Project. J. Geophys. Res. 97, 11703. https://doi.org/10.1029/92JB00132.
Zuffetti, C., Bersezio, R., 2020. Morphostructural evidence of late Quaternary tectonics at the Po Plain-Northern Apennines border (Lombardy, Italy). Geomorphology 364, 107245. https://doi.org/10.1016/j.geomorph.2020.107245.
Zuffetti, C., Bersezio, R., Contini, D., Petrizzo, M.R., 2018a. Geology of the San Colombano hill, a Quaternary isolated tectonic relief in the Po Plain of Lombardy (Northern Italy). Journal of Maps 14, 199–211. https://doi.org/10.1080/17445647.2018.1443166.
Zuffetti, C., Trombino, L., Zembo, I., Bersezio, R., 2018b. Soil evolution and origin of landscape in a late Quaternary tectonically mobile setting: the Po Plain-Northern Apennines border in Lombardy (Italy). CATENA 171, 376–397. https://doi.org/10.1016/j.catena.2018.07.026.